

Global and local condensate and superfluid fractions of a few hard core Bosons in a combined harmonic optical cubic lattice

Asaad R. Sakhel¹

¹*Al-Balqa Applied University, Faculty of Engineering Technology,
Applied Sciences Department, Amman 11134, JORDAN*

(Dated: October 21, 2018)

We explore the global and local condensate and superfluid (SF) fractions in a system of a few hard core (HC) bosons ($N = 8$ and $N = 40$) trapped inside a combined harmonic optical cubic lattice (CHOCL) at $T = 0$ K. The condensate fraction (CF) is computed for individual lattice wells by separating the one-body density matrix (OBDM) of the whole system into components at the various lattice sites. Then each “lattice-site” component is diagonalized to find its eigenvalues. The eigenvalues are obtained by a method presented earlier [Dubois and Glyde, Phys. Rev. A **63**, 023602 (2001)]. The effects of interference between the condensates in the lattice wells on the CF in one well is also investigated. The SF fraction (SFF) is calculated for $N = 40$ by using the diffusion formula of Pollock and Ceperley [Pollock and Ceperley, Phys. Rev. B **36**, 8343 (1987)]. Our chief result is an opposing behavior of the global CF and SFF with increasing lattice wave vector k . In addition, the CF in a lattice well is enhanced by the interference with its neighbor wells beyond the result when the interference is neglected. The global SF is depleted with a rise of the repulsion between the bosons, yet at very strong interaction superfluidity is still present. The global CF remains almost constant with increasing HC repulsion. A reduction in the lattice dimension, i.e. an increase in the lattice wave vector, increases the local CF in each lattice well, but reduces the corresponding local SFF. At large HC repulsion, a coexisting SF-(vacuum)MI phase is established.

PACS numbers: 67.85.-d,67.85.Hj,03.75.-b,03.75.Lm

I. INTRODUCTION

The Bose-Einstein condensation (BEC) of bosons in optical lattices (OLs) has recently become a topic of great interest which motivated substantial work [1–12]. Interesting investigations included an experimental realization of the latter [1], BECs in tight binding bands of OLs with different geometries [6], the Bose-Hubbard model (BHM) [12–15], effects of the lattice dimension [16], and instabilities of BECs in moving two-dimensional (2D) OLs [4].

A topic of importance is the measurement of the condensate fraction (CF) in individual OL wells, for which only a few investigations have been reported [3, 17, 18]. Investigations concentrated mostly on measuring the *total* CF of the whole lattice system. For example, in a 2D lattice boson system, Spielman *et al.* [19] experimentally measured the CF of Rb atoms as a function of the lattice depth. Furthermore, Fang *et al.* [10] measured the CF of a ⁸⁷Rb gas released from an OL in a time-of-flight (TOF) experiment.

Importantly, Chen and Wu [4] noted that most of the theoretical work focused only on BECs in 1D OLs, and that the literature on 2D and three-dimensional (3D) OLs is still scarce. We were thus motivated to explore BECs in 3D OLs; the work of Brouzos *et al.* [18] provides also the chief motivation.

According to Chen and Wu [4], a BEC confined in a strong 1D lattice can be regarded as a chain of weakly coupled condensate islands trapped in the lattice wells. This idea has also been propagated by Shams and Glyde [20] and there would be little tunneling between these islands, as Chen and Wu stated. Our upcoming formula-

tion of the present problem is based on the latter thought. That is, we study the role of the interference between the condensate in one lattice well and the condensates in all-neighbor wells. In this regard, we were also motivated by the work of Baillie and Blackie [21].

Further, superfluidity in OLs has also been given considerable interest [3, 17, 22–25]. Particularly the superfluid (SF) to Mott-insulator (MI) transition [24, 26–34] has been explored intensively ever since its first experimental realization [22], as well as coexisting SF and MI domains of harmonically trapped hard core (HC) and lattice bosons [14, 15, 33, 35, 36]. For example, Roth and Burnet [24], used a twisted-boundary condition approach to compute the superfluid fraction (SFF) in a one-dimensional (1D) lattice. Similarly, Hen and Rigol [26] applied a twist in the boundary conditions to evaluate the SFF of HC bosons in a superlattice. The twist in the boundary conditions can, however, be only applied to a homogeneous OL system. In addition, using the BHM, the effects of an external harmonic trap on the state diagram of lattice bosons have been explored by Rigol *et al.* [14], specifically for the coexistence of MI and SF domains inside the system. The vanishing of the CF at large values of the lattice depth indicated also the crossing from the SF to the MI domain [19].

The role of the HC diameter in the SF and condensate depletion of hard sphere (HS) bosons in OLs has, to the best of our knowledge, rarely been outlined before, particularly in the SF-MI transition of a few-body system. So far, the investigations of the CF and SFF have been largely as functions of the lattice barrier (c.f. Shams and Glyde [20] and Spielman *et al.* [19]); in con-

trast we explore them as functions of the boson HC interactions. One of the few investigations on the role of the interactions in the condensate properties inside an OL was undertaken by Snoek *et al.* [37] and Ramanan *et al.* [33] for a 1D Bose gas in an inhomogeneous OL. Snoek *et al.* explored the effect of interactions on the condensate properties of a Bose-Fermi mixture trapped in a 3D harmonic OL. Among their findings, was that the condensate is depleted with a rise of the Bose-Fermi repulsive interactions which are similar to the boson HC interactions. Whereas Snoek *et al.* conducted their calculations for the whole of their system, we explore the condensate at individual lattice sites and then sum all individual contributions.

One important investigation most relevant to ours was presented by Brouzos *et al.* [18], who conducted studies on homogeneous few-particle bosonic systems in a 1D multiwell trap. Some of our findings for a 3D OL are similar to theirs. Further, the latter authors articulated that exact studies of trapped bosonic systems “are particular for a few number of particles”. Few particles have also been used, e.g. by Fang *et al.* [10] who did calculations on a 1D Bose gas in an OL with only ten particles in ten lattice sites. We shall devote a special section for connecting our results with the findings of Ref.[18] later on below.

In our work here, the CF and SFF of a few HC bosons trapped inside a combined harmonic optical cubic lattice (CHOCL) is studied at $T = 0$ K. The cubic OL has $3 \times 3 \times 3$ lattice sites, or lattice wells. Most importantly, the nonspherical symmetry of the CHOCL system is dealt with which poses a difficulty for the computation of its global CF. This fact has been outlined recently by Astrakharchik and Krutitsky [38], who presented a method for the calculation of the total CF of an inhomogeneous Bose gas confined by an OL. Yet this work here proposes to evaluate the CF in each individual lattice well. Hence, another goal of our paper is to present methods for computing the CF and SFF in each well of the CHOCL system. The total CF and SFF are also computed. An important point to emphasize, is that we distinguish clearly between global and local CF and SFF. Motivated by the work of Xue *et al.* [16], we also decided to check the role of the lattice dimension on the properties of the CF and SFF. In another attempt, we seek a MI state in our systems by going to large HC repulsions and OL depths. We also make a clear distinction between the effects of repulsive forces with *zero range*, as encountered in the BHM, and repulsive forces with a *nonzero* range, as described by the HS Jastrow function, Eq.(5) below. A pair of bosons interacting solely by a repulsive delta function can still be brought close to each other by external forces; but if they are HSs, then their closest distance of approach is a_c below which they face an infinite hard-wall barrier.

The current paper comes as a continuation to the investigation of the properties of HC bosons in a CHOCL by Sakhel *et al.* [39], in continuous space and for a few-

body system. This is in an attempt to provide further manifestation of the condensate properties inside an OL. Therefore we ask ourselves various questions: Will an increase of the HC diameter deplete the SF or BEC inside the CHOCL in the case of a few bosons? Can we realize a MI by increasing the HC diameter to large values instead of the OL depth? What is the effect of interference between the condensates in all lattice wells on the condensate in one well? We also would like to emphasize that the current investigation provides further evidence for the presence of superfluidity in a 3D CHOCL. Previously, Sun *et al.* [3] presented striking experimental evidence for the presence of SF states in a shallow OL. Sun *et al.* [3] found that the CF in a deep lattice is significantly lower than 1. Further, in a shallow limit, the SFF is 100% [3]. Correspondingly, our findings here indicate an overall CF of the order of $\sim 100\%$ in the weakly-interacting regime for $N = 8$ particles and an OL of depth $V_0 = 10$ (in trap units). On the other hand, the SFF is $\sim 90\%$ in the weakly-interacting regime for $V_0 = 10$ and $N = 40$ particles (see Fig. 8).

The key findings of this paper are as follows: i) the most important result is an opposing behavior of the global CF and SFF as functions of the lattice spacing. Whereas a reduction in the lattice spacing decreases the global SFF, it leads at the same time to an increase in the CF of the whole system. This is counter-intuitive and arises from a distinction between local condensate density and global SF density; ii) the SFF is reduced with a rise of the HC diameter in correspondence to a decline in the single-particle tunneling, earlier reported by Sakhel *et al.*; iii) the interference between the condensates in all lattice wells enhances the CF in each well beyond the result without interference effects; iv) the energy rises with increasing HC diameter whereas the SFF declines. As a result, one can conclude that the rise in the energy is mostly due to a buildup of the onsite repulsive energy in each lattice well which overtakes the drop in the boson mobility; v) for a small number of HC bosons N inside a CHOCL with a limited number of lattice sites N_L , it is possible to achieve a mixed SF-MI state. vi) the local and global CF, and SFF, are distinct quantities. vii) the principle factor in depleting a BEC in a CHOCL with few bosons is the OL.

The paper is organized as follows. In Sec.II, we outline the methods used for the evaluation of the CF and SFF. In Sec.III, we present our results and discuss them, and in Sec.IV we present our conclusions.

II. METHOD

In this section, we describe the methods used in the evaluation of the local and global CF and SFF in each lattice well, as well as the global CF and SFF. We consider N HC bosons confined by a CHOCL of $3 \times 3 \times 3$ sites. The local CF is computed by separating the one-body density matrix (OBDM) of the whole system into

its components centered at the various lattice sites. By treating the distribution of particles in each lattice well as a spherically symmetric cloud (we show justification for this), we diagonalize the OBDM components and find their corresponding eigenvalues for a particular number of sites representative of the whole OL. This is performed for two cases, one involving no interference between the condensate clouds in all lattice wells, and the other with this interference included. The global CF is then obtained by summing the contributions from individual lattice wells. The local SFF is evaluated by dividing the large cubic OL volume into 27 small cubes of edge d , and computing the SFF within the boundaries of each small cube. The global SFF is computed as well, and for both local and global SFF a winding-number like formula is applied.

For the purpose of evaluating the OBDM and the associated eigenvalues, we modified a previously written code by Dubois and Glyde [40]. For the evaluation of the SFF, we applied the diffusion formula of Pollock and Ceperley [41]. The variational path integral Monte Carlo (VPI) method [42, 43] was used to evaluate the SFF of the systems treated in Ref.[39]. We used quantum variational Monte Carlo (VMC) to compute the spatial configurations of the particles in the current systems from which the OBDMs are obtained.

A. Hamiltonian

The Hamiltonian of the system is given by

$$H = -\frac{\hbar^2}{2m} \sum_{i=1}^N \nabla_i^2 + \sum_{i=1}^N [V_{ho}(\mathbf{r}_i) + V_{opt}(\mathbf{r}_i)] + \sum_{i<j} V_{int}(\mathbf{r}_i - \mathbf{r}_j), \quad (1)$$

where $V_{ho}(\mathbf{r}_i) = \frac{1}{2}m\omega_{ho}^2 r_i^2$ is the harmonic oscillator (HO) trapping potential, with $\mathbf{r}_i \equiv (x_i, y_i, z_i)$ the position of a particle from the center of this trap, m the mass of the particle, and ω_{ho} the trapping frequency. Upon this trap, there is superimposed an OL potential

$$V_{opt}(\mathbf{r}_i) = V_0 [\sin^2(k_x x_i) + \sin^2(k_y y_i) + \sin^2(k_z z_i)], \quad (2)$$

with V_0 the height of the OL barrier, and $k_i = \pi/d$ ($i \equiv x, y, \text{ or } z$) is the lattice wave vector with d the lattice spacing. For further details refer to Ref.[39]. The interparticle interactions are given by the hard sphere (HS) potential

$$V_{int}(r_{ij}) = \begin{cases} \infty & ; \quad r_{ij} \leq a_c \\ 0 & ; \quad r_{ij} > a_c \end{cases}, \quad (3)$$

where a_c is the HC diameter of the bosons, and $r_{ij} \equiv |\mathbf{r}_i - \mathbf{r}_j|$ is the interparticle distance between two bosons

i and j . a_c equals the s-wave scattering length in the low-energy and long-wavelength approximation of the two-particle scattering problem.

B. Density matrix and CF at a lattice site

We begin with the VMC trial wave function of a previous publication [39] given by

$$\Psi(\{\mathbf{r}\}, \{\mathbf{R}\}) = \prod_{i=1}^N \exp(-\alpha r_i^2) \psi(\mathbf{r}_i, \{\mathbf{R}\}) \prod_{i<j} f(|\mathbf{r}_i - \mathbf{r}_j|), \quad (4)$$

where $f(|\mathbf{r}_i - \mathbf{r}_j|)$ is the HS Jastrow function [40]

$$f(r) = 1 - \frac{a_c}{r}, \quad (5)$$

with a_c the HC diameter of the bosons. An important condition is that $f(r) = 0$ if $r \leq a_c$. Here $\{\mathbf{r}\} \equiv (\mathbf{r}_1, \mathbf{r}_2, \dots, \mathbf{r}_N)$ is the set of N particle positions, and $\{\mathbf{R}\} \equiv (\mathbf{R}_1, \mathbf{R}_2, \dots, \mathbf{R}_{N_L})$ the set of N_L lattice site positions, where $\mathbf{R}_n \equiv (i\mathbf{i} + j\mathbf{j} + k\mathbf{k})\pi/d$ and is abbreviated $\mathbf{R}_n \equiv (ijk)$. The index n runs from 1 to N_L , where N_L is the total number of lattice sites (here 27). Eq.(4) is then optimized with respect to its parameters [α of Eq.(4) above, and β , γ , and σ of Eq.(7) below] as outlined previously [39]. By using the Wannier-like function defined by

$$\psi(\mathbf{r}_i, \{\mathbf{R}\}) = \sum_{n=0}^{N_L} \phi(\mathbf{r}_i, \mathbf{R}_n), \quad (6)$$

with $\phi(\mathbf{r}_i, \mathbf{R}_n)$ given by

$$\begin{aligned} \phi(\mathbf{r}_i, \mathbf{R}_n) = & \exp[-\beta(\mathbf{r}_i - \mathbf{R}_n)^2] \times \\ & [1 + \gamma(x_i - X_n)^2 - \sigma(x_i - X_n)^4] \times \\ & [1 + \gamma(y_i - Y_n)^2 - \sigma(y_i - Y_n)^4] \times \\ & [1 + \gamma(z_i - Z_n)^2 - \sigma(z_i - Z_n)^4], \end{aligned} \quad (7)$$

we consider expanding the OBDM into its components at each lattice site of position \mathbf{R}_n .

To set the stage, we start out by evaluating the total density matrix

$$\begin{aligned} \rho(\mathbf{r}_1, \mathbf{r}'_1) = & \int d\mathbf{r}_2 d\mathbf{r}_3 \dots d\mathbf{r}_N \Psi^*(\mathbf{r}_1, \mathbf{r}_2, \dots, \mathbf{r}_N, \{\mathbf{R}\}) \times \\ & \Psi(\mathbf{r}'_1, \mathbf{r}_2, \dots, \mathbf{r}_N, \{\mathbf{R}\}), \end{aligned} \quad (8)$$

using the standard Monte Carlo integration approach [44]

$$\rho(\mathbf{r}_1, \mathbf{r}'_1) = \frac{1}{P} \sum_{c=1}^P \Psi^*(\mathbf{r}_1, \mathbf{r}_{c2}, \dots, \mathbf{r}_{cN}, \{\mathbf{R}\}) \times \frac{1}{w_c} \Psi^*(\mathbf{r}'_1, \mathbf{r}_{c2}, \dots, \mathbf{r}_{cN}, \{\mathbf{R}\}) \times \frac{1}{P} \sum_{c=1}^P \frac{\prod_{1 < j} f(|\mathbf{r}'_1 - \mathbf{r}_{cj}|)}{\prod_{1 < j} f(|\mathbf{r}_1 - \mathbf{r}_{cj}|)}. \quad (12)$$

where w_c is a configurational weight to be determined later, and P is the number of Monte Carlo configurations. The subscript c in \mathbf{r}_{ci} labels the configuration to which particle i belongs. Since according to Eq.(6) $\Psi(\{\mathbf{r}\}, \{\mathbf{R}\})$ is a sum over all lattice sites, we can expand $\rho(\mathbf{r}_1, \mathbf{r}'_1)$ [Eq.(9)] into a sum of components at positions \mathbf{R}_n . The latter sum $\rho(\mathbf{r}_1, \mathbf{r}'_1)$ involves interference components between one at \mathbf{R}_q and all other lattice sites $\mathbf{R}_{n \neq q}$. In this study we are concerned with both interfering and noninterfering ones. On substituting (4) and (6) into (9), one gets

$$\begin{aligned} \rho(\mathbf{r}'_1, \mathbf{r}_1) &= e^{-\alpha r_1^2} e^{-\alpha r_1'^2} \times \\ &\left[\sum_{n=1}^{N_L} \phi(\mathbf{r}_1, \mathbf{R}_n) \right] \left[\sum_{n=1}^{N_L} \phi(\mathbf{r}'_1, \mathbf{R}_n) \right] \times \\ &\frac{1}{P} \sum_{c=1}^P \frac{1}{w_c} \prod_{1 < j} f(|\mathbf{r}_1 - \mathbf{r}_{cj}|) \prod_{1 < j} f(|\mathbf{r}'_1 - \mathbf{r}_{cj}|) \times \\ &\left\{ \prod_{i \neq 1}^N e^{-\alpha r_{ci}^2} \left[\sum_{n=1}^{N_L} \phi(\mathbf{r}_{ci}, \mathbf{R}_n) \right] \prod_{i < j, i \neq 1}^N f(|\mathbf{r}_{ci} - \mathbf{r}_{cj}|) \right\}^2. \end{aligned} \quad (10)$$

Let us now choose the configurational weight to be of the form

$$\begin{aligned} w_c &= |\Psi[(\mathbf{r}_1, \mathbf{r}_{c2}, \dots, \mathbf{r}_{cN}), \{\mathbf{R}\}]|^2 \\ &= e^{-2\alpha r_1^2} \left[\sum_{n=1}^{N_L} \phi(\mathbf{r}_1, \mathbf{R}_n) \right]^2 \left[\prod_{1 < j} f(|\mathbf{r}_1 - \mathbf{r}_{cj}|) \right]^2 \times \\ &\prod_{i \neq 1}^N e^{-2\alpha r_{ci}^2} \left[\sum_{n=1}^{N_L} \phi(\mathbf{r}_{ci}, \mathbf{R}_n) \right]^2 \left[\prod_{i < j, i \neq 1} f(|\mathbf{r}_{ci} - \mathbf{r}_{cj}|) \right]^2, \end{aligned} \quad (11)$$

which has been chosen in a previous publication [39]. Substituting this weight into (10), the exponentials and Jastrow terms $f(|\mathbf{r}_{ci} - \mathbf{r}_{cj}|)$ cancel out, and one remains with

$$\begin{aligned} \rho(\mathbf{r}'_1, \mathbf{r}_1) &= \frac{e^{-\alpha r_1'^2}}{e^{-\alpha r_1^2}} \times \\ &\frac{\left[\sum_{n=1}^{N_L} \phi(\mathbf{r}_1, \mathbf{R}_n) \right] \left[\sum_{n=1}^{N_L} \phi(\mathbf{r}'_1, \mathbf{R}_n) \right]}{\left[\sum_{n=1}^{N_L} \phi(\mathbf{r}_1, \mathbf{R}_n) \right]^2} \times \end{aligned}$$

1. Interfering and noninterfering components of the OBDM

In what follows, we shall separate the density matrix $\rho(\mathbf{r}_1, \mathbf{r}'_1)$ into interfering and noninterfering (isolated-islands) components. First, the numerator in the second line of Eq.(12) is rewritten

$$\begin{aligned} &\left[\sum_{n=1}^{N_L} \phi(\mathbf{r}_1, \mathbf{R}_n) \right] \left[\sum_{q=1}^{N_L} \phi(\mathbf{r}'_1, \mathbf{R}_q) \right] = \\ &\sum_{n=1}^{N_L} \left[\phi(\mathbf{r}_1, \mathbf{R}_n) \phi(\mathbf{r}'_1, \mathbf{R}_n) + \sum_{q \neq n}^{N_L} \phi(\mathbf{r}_1, \mathbf{R}_n) \phi(\mathbf{r}'_1, \mathbf{R}_q) \right], \end{aligned} \quad (13)$$

where the first term in the second line of (13) is the noninterfering ($n = q$) part describing isolated clouds, and the second term the interfering part ($q \neq n$), respectively. Next, by using (13) in (12), the total density matrix can be written as the sum of two components

$$\begin{aligned} \rho(\mathbf{r}_1, \mathbf{r}'_1) &= \sum_{n=1}^{N_L} \rho^{(0)}(\mathbf{r}_1 - \mathbf{R}_n, \mathbf{r}'_1 - \mathbf{R}_n) + \\ &\sum_{n=1}^{N_L} \rho^{(1)}(\mathbf{r}_1 - \mathbf{R}_n, \mathbf{r}'_1 - \mathbf{R}_n), \end{aligned} \quad (14)$$

where we define the noninterfering density matrix for each ‘‘isolated’’ cloud at a lattice site \mathbf{R}_n as

$$\begin{aligned} \rho^{(0)}(\mathbf{r}_1 - \mathbf{R}_n, \mathbf{r}'_1 - \mathbf{R}_n) &= \\ e^{-\alpha r_1'^2} e^{\alpha r_1^2} \frac{\phi(\mathbf{r}_1, \mathbf{R}_n) \phi(\mathbf{r}'_1, \mathbf{R}_n)}{\left[\sum_{q=1}^{N_L} \phi(\mathbf{r}_1, \mathbf{R}_q) \right]^2} J(\mathbf{r}'_1, \mathbf{r}_1), \end{aligned} \quad (15)$$

and the density matrix involving interference components only ($n \neq q$) as

$$\begin{aligned} \rho^{(1)}(\mathbf{r}_1 - \mathbf{R}_n, \mathbf{r}'_1 - \mathbf{R}_n) &= \\ e^{-\alpha r_1'^2} e^{\alpha r_1^2} \frac{\phi(\mathbf{r}_1, \mathbf{R}_n) \sum_{q \neq n}^{N_L} \phi(\mathbf{r}'_1, \mathbf{R}_q)}{\left[\sum_{q=1}^{N_L} \phi(\mathbf{r}_1, \mathbf{R}_q) \right]^2} J(\mathbf{r}'_1, \mathbf{r}_1). \end{aligned} \quad (16)$$

For brevity, we have defined the term involving Jastrow functions as

$$J(\mathbf{r}'_1, \mathbf{r}_1) = \frac{1}{P} \sum_{c=1}^P \frac{\prod_{1 < j} f(|\mathbf{r}'_1 - \mathbf{r}_{cj}|)}{\prod_{1 < j} f(|\mathbf{r}_1 - \mathbf{r}_{cj}|)}. \quad (17)$$

Note that the order in which the sums of $\phi(\mathbf{r}_i, \mathbf{R}_n)$ in Eq.(12) are multiplied and divided is very important to obtain Eqs.(15) and (16). First, we evaluated the numerator (13) by extracting out the interfering ($n \neq q$) and noninterfering terms ($n = q$). Second, we divided by the denominator $\left[\sum_{n=1}^{N_L} \phi(\mathbf{r}_1, \mathbf{R}_n) \right]^2$. Yet if we considered first canceling out the summation $\sum_{n=1}^{N_L} \phi(\mathbf{r}_1, \mathbf{R}_n)$ in the numerator of the second line of Eq.(12), with one power of the sum in the denominator, we would get a different result given by Eq.(30) next.

2. Eigenvalues of the CHOCL-OBDM components

Assuming now the cloud at each lattice site to be spherical, we utilize in what follows the recipe of Dubois and Glyde [40], which is for the evaluation of the CF in an isotropic harmonic trap, to compute the CF in each lattice well. Let us first consider the noninterfering case. First, one begins by expanding the density matrix (15) at lattice site \mathbf{R}_n into angular momentum components as follows:

$$\rho^{(0)}(\mathbf{r}_1 - \mathbf{R}_n, \mathbf{r}'_1 - \mathbf{R}_n) = \sum_{\ell=0}^{\infty} \frac{(2\ell+1)}{4\pi} P_{\ell}(u_{\mathbf{r}_1, \mathbf{r}'_1}^{(n)}) \rho_{\ell}^{(0)}(|\mathbf{r}_1 - \mathbf{R}_n|, |\mathbf{r}'_1 - \mathbf{R}_n|), \quad (18)$$

where $P_{\ell}(x)$ is the Legendre polynomial of order ℓ and

$$u_{\mathbf{r}_1, \mathbf{r}'_1}^{(n)} = \frac{(\mathbf{r}_1 - \mathbf{R}_n) \cdot (\mathbf{r}'_1 - \mathbf{R}_n)}{|\mathbf{r}_1 - \mathbf{R}_n| |\mathbf{r}'_1 - \mathbf{R}_n|}, \quad (19)$$

the cosine of the angle between $(\mathbf{r}_1 - \mathbf{R}_n)$ and $(\mathbf{r}'_1 - \mathbf{R}_n)$. The $\rho_{\ell}^{(0)}$ corresponds to the angular momentum component of $\rho^{(0)}$ and is obtained by multiplying both sides of (18) by $P_{\ell}(u_{\mathbf{r}_1, \mathbf{r}'_1}^{(n)})$ and integrating over the solid-angle element $d\Omega_1 = 2\pi \sin \gamma d\gamma$, considering that $\cos \gamma = u_{\mathbf{r}_1, \mathbf{r}'_1}^{(n)}$. This yields

$$\rho_{\ell}^{(0)}(|\mathbf{r}_1 - \mathbf{R}_n|, |\mathbf{r}'_1 - \mathbf{R}_n|) = \int d\Omega_1 P_{\ell}(u_{\mathbf{r}_1, \mathbf{r}'_1}^{(n)}) \rho^{(0)}(\mathbf{r}_1 - \mathbf{R}_n, \mathbf{r}'_1 - \mathbf{R}_n), \quad (20)$$

where the orthogonality condition for Legendre polynomials [45] has been applied:

$$\int_0^{\pi} P_{\ell}(\cos \gamma) P_{\ell'}(\cos \gamma) \sin \gamma d\gamma = \frac{2\delta_{\ell\ell'}}{2\ell+1}, \quad (21)$$

with $\delta_{\ell\ell'}$ the Kronecker delta function.

Second, one defines the local natural orbitals (LNOs) and diagonalizes the local OBDM to evaluate the eigenvalues of the OBDM in each well. Hence, similarly to Dubois and Glyde [40] one first redefines the local non-interfering density matrix (18) using their field-operator approach:

$$\rho^{(0)}(\mathbf{r}_1 - \mathbf{R}_n, \mathbf{r}'_1 - \mathbf{R}_n) = \langle \hat{\Psi}_0^{\dagger}(\mathbf{r}_1 - \mathbf{R}_n) \hat{\Psi}_0(\mathbf{r}'_1 - \mathbf{R}_n) \rangle, \quad (22)$$

$\hat{\Psi}_0(\mathbf{r}_1 - \mathbf{R}_n)$ being a local field operator which annihilates a particle at position $\mathbf{r}_1 - \mathbf{R}_n$. Then one expands $\hat{\Psi}_0(\mathbf{r}_1 - \mathbf{R}_n)$ into a set of local single particle states $\chi_i(\mathbf{r}_1 - \mathbf{R}_n)$ around \mathbf{R}_n :

$$\hat{\Psi}_0(\mathbf{r}_1 - \mathbf{R}_n) = \sum_{i=1}^N \chi_i(\mathbf{r}_1 - \mathbf{R}_n) \hat{a}_i^{(n)}, \quad (23)$$

$\hat{a}_i^{(n)}$ being a bosonic annihilation operator acting inside well n at position \mathbf{R}_n . The χ_i are taken to be orthonormal such that

$$\int d\mathbf{r}_1 \chi_i^*(\mathbf{r}_1 - \mathbf{R}_n) \chi_j(\mathbf{r}_1 - \mathbf{R}_n) = \delta_{ij}. \quad (24)$$

Substituting (23) into (22) above, and using the usual condition $\langle \hat{a}_i^{(n)\dagger} \hat{a}_j^{(n)} \rangle = N_i^{(n)} \delta_{ij}$, one gets

$$\rho^{(0)}(\mathbf{r}_1 - \mathbf{R}_n, \mathbf{r}'_1 - \mathbf{R}_n) = \sum_{ij} \chi_i^*(\mathbf{r}_1 - \mathbf{R}_n) \chi_j(\mathbf{r}'_1 - \mathbf{R}_n) N_i^{(n)} \delta_{ij}, \quad (25)$$

Multiplying both sides of (25) by $\chi_j(\mathbf{r}_1 - \mathbf{R}_n)$ from the left and $\chi_i^*(\mathbf{r}'_1 - \mathbf{R}_n)$ from the right, then integrating over \mathbf{r}_1 and \mathbf{r}'_1 , this yields

$$\int d\mathbf{r}_1 d\mathbf{r}'_1 \chi_j(\mathbf{r}_1 - \mathbf{R}_n) \rho^{(0)}(\mathbf{r}_1 - \mathbf{R}_n, \mathbf{r}'_1 - \mathbf{R}_n) \times \chi_i^*(\mathbf{r}'_1 - \mathbf{R}_n) = N_i \delta_{ij}. \quad (26)$$

The eigenvectors $\chi_i(\mathbf{r}_1 - \mathbf{R}_n)$ are the LNOs with eigenvalues $N_i^{(n)}$. Making now use of the spherical symmetry of the system, one further defines

$$\chi_i(\mathbf{r}_1 - \mathbf{R}_n) = \xi_{q\ell}(|\mathbf{r}_1 - \mathbf{R}_n|) Y_{\ell m}(\theta, \varphi), \quad (27)$$

$i \equiv (q\ell m)$ being a state, $\xi_{q\ell}(|\mathbf{r}_1 - \mathbf{R}_n|)$ being the local radial wave function, and $Y_{\ell m}(\theta, \varphi)$ the spherical harmonic function with θ and φ defining the angular position of

$\mathbf{r}_1 - \mathbf{R}_n$. It must be noted, that in $N_i^{(n)}$ we drop the quantum number m so that $N_i^{(n)} = N_{q\ell}^{(n)}$ because of azimuthal symmetry in each well. Substituting (27) and (18) into (25), using the addition theorem for Legendre polynomials [45]

$$P_\ell(\cos \gamma) = \frac{4\pi}{2\ell + 1} \sum_{m=-\ell}^{m=+\ell} Y_{\ell m}(\theta, \varphi) Y_{\ell m}^*(\theta', \varphi') \quad (28)$$

with

$$\cos \gamma = \sin \theta \sin \theta' \cos(\varphi - \varphi') + \cos \theta \cos \theta',$$

and the orthogonality condition (21), this eventually yields the expansion of the angular momentum component (20) into the radial functions $\xi_{q\ell}$

$$\begin{aligned} \rho_\ell^{(0)}(|\mathbf{r}_1 - \mathbf{R}_n|, |\mathbf{r}'_1 - \mathbf{R}_n|) = \\ \sum_q \xi_{q\ell}(|\mathbf{r}_1 - \mathbf{R}_n|) \xi_{q\ell}(|\mathbf{r}'_1 - \mathbf{R}_n|) N_{q\ell}^{(n)}, \end{aligned} \quad (29)$$

where $N_{q\ell}^{(n)}$ are the eigenvalues of the natural orbitals $\chi_i(\mathbf{r}_1 - \mathbf{R}_n)$ at lattice site n and positions $\mathbf{R}_n \equiv (ijk)$. As such, the natural orbital $\chi_0(\mathbf{r}_1 - \mathbf{R}_n)$ whose eigenvalue is $N_{00}^{(n)}$, is defined as the condensate orbital. $N_{00}^{(n)}/N$ is then the CF at site n and position \mathbf{R}_n with respect to the overall number of particles N . One then proceeds similarly to Dubois and Glyde [40] in the diagonalization of the OBDM in order to compute the eigenvalues $N_{q\ell}^{(n)}$, and consequently the CF, except that we do this here for one lattice site at a time.

By considering the additional interference between a condensate at lattice site \mathbf{R}_n and all-neighbor lattice sites $\mathbf{R}_q \neq \mathbf{R}_n$, the CF at lattice site \mathbf{R}_n is computed using the same previous procedure, except that we use all terms of the density matrix (12) which contains the interference between the condensates at the various lattice sites, instead of the noninterfering $\rho^{(0)}$ only. That is, one writes

$$\begin{aligned} \rho(\mathbf{r}_1 - \mathbf{R}_n, \mathbf{r}'_1 - \mathbf{R}_n) = e^{-\alpha r_1'^2} e^{\alpha r_1^2} \times \\ \frac{\phi(\mathbf{r}'_1, \mathbf{R}_n)}{\left| \sum_{q=1}^{N_L} \phi(\mathbf{r}_1, \mathbf{R}_q) \right|} J(\mathbf{r}'_1, \mathbf{r}_1), \end{aligned} \quad (30)$$

where $\rho = \rho^{(0)} + \rho^{(1)}$. Consequently, Eqs.(18), (20), and (29) are simply rewritten by replacing $\rho^{(0)}$ with ρ in all terms. Eventually, one gets instead of (29)

$$\begin{aligned} \rho_\ell(|\mathbf{r}_1 - \mathbf{R}_n|, |\mathbf{r}'_1 - \mathbf{R}_n|) = \\ \sum_q \widetilde{\xi}_{q\ell}(|\mathbf{r}_1 - \mathbf{R}_n|) \widetilde{\xi}_{q\ell}(|\mathbf{r}'_1 - \mathbf{R}_n|) \widetilde{N}_{q\ell}^{(n)}, \end{aligned} \quad (31)$$

where $\widetilde{N}_{q\ell}^{(n)}$ and $\widetilde{\xi}_{q\ell}$ are similar to $N_{q\ell}^{(n)}$ and $\xi_{q\ell}$, but including contributions from the interference with all-neighbor lattice sites.

C. Definitions of CF in our systems

To set the stage, we define $n_{(ijk)} = N_{00}^{(n)}/N$ to be the CF in the lattice well centered at $\mathbf{R}_n \equiv (ijk)$ with respect to the total number of particles N , and *without* all-well interference, and $\widetilde{n}_{(ijk)} = \widetilde{N}_{00}^{(n)}/N$ as the corresponding CF *with* all-neighbor interference, labelled by a star in each upcoming figure legend. The $n_{(ijk)}$ and $\widetilde{n}_{(ijk)}$ are computed as explained in Sec.II B.

Hence $n_{(000)}$ is the fraction of particles in the lowest orbital of the central cell, $n_{(010)}$ that of cell (010), etc. In fact, the natural orbital is spread out over the entire lattice and is not localized in one lattice site. That is, one has a lowest orbital at all lattice sites (ijk) if they display a CF. This spreading is a Wannier sum over individual-cell natural orbitals. Since the CF at site (ijk) is with respect to the total number of particles N , the total CF of the system in the $3 \times 3 \times 3$ cubic lattice can be computed using

$$\begin{aligned} n_0 = \sum_{ijk} n_{(ijk)} \approx \\ n_{(000)} + 6 n_{(010)} + 12 n_{(011)} + 8 n_{(111)}. \end{aligned} \quad (32)$$

Note that $n_{(010)}$ is ideally identical to $n_{(001)}$, $n_{(100)}$, $n_{(-100)}$, etc. Similarly $n_{(011)}$ is equal to $n_{(101)}$, $n_{(110)}$, $n_{(-110)}$, etc; the same holds for $n_{(111)}$. The large cube divided into $3 \times 3 \times 3$ smaller equal-sized cubes has 6 lattice sites at its face-centers, 8 at the corners, and 12 at the bisecting points of its edges.

The CF in each lattice well is then explored as a function of a_c for the three lattice wave vectors $k = \pi$, 1.2π , and 1.4π . The latter results are compared with the corresponding CF $\widetilde{n}_{(ijk)}$.

D. Superfluid fraction

The global SFF is computed using the variational path integral Monte Carlo (VPI) technique [42, 43] via the diffusion formula of Pollock and Ceperely [41]:

$$\frac{\rho_s}{\rho} = \frac{D_p}{D_0}, \quad (33)$$

where $D_0 = \hbar^2/(2m)$ is the ‘‘quantum diffusion’’ constant and

$$D_p = \frac{1}{2d\beta N} \left\langle \left[\sum_{i=1}^N (\mathbf{r}_i - \mathbf{r}_{Mi}) \right]^2 \right\rangle, \quad (34)$$

with d the dimensionality of the system, N the number of particles, imaginary time $\beta \leftrightarrow 1/(k_B T)$ with k_B the Boltzmann constant, and T the temperature. Here $\langle \dots \rangle$ denotes a configurational Monte Carlo average, \mathbf{r}_i is the

initial position of a particle i , and \mathbf{r}_{Mi} the destination of the particle after a “time” β , where M is the number of VPI time slices. In this regard, we evaluate the configurational average D_p over a number P of VPI configurations:

$$D_{p,VPI} = \frac{1}{2d\beta N} \frac{1}{P} \sum_{c=1}^P \left[\sum_{i=1}^N (\mathbf{r}_{ci} - \mathbf{r}_{Mci}) \right]^2. \quad (35)$$

For $d = 3$, and using units of the trap $a_{ho} = \sqrt{\hbar/(m\omega_{ho})}$ and $\hbar\omega_{ho}$ for length and energy, respectively, the SFF is then recast into the form

$$n_s = \frac{\rho_s}{\rho} = \frac{1}{3M\tau} \frac{1}{NP} \sum_{c=1}^P \left[\sum_{i=1}^N (\mathbf{r}_{ci} - \mathbf{r}_{Mci}) \right]^2, \quad (36)$$

where $\mathbf{r} \rightarrow \mathbf{r}/a_{ho}$, $\beta \rightarrow \beta\hbar\omega_{ho}$, and $\tau \rightarrow \beta\hbar\omega_{ho}/M = \hbar\omega_{ho}/(Mk_B T)$ is the “time step” with M the number of time slices. We would also like to remind the reader that we are aiming at presenting qualitative rather than quantitative results. The parameters used were $M = 120$, $\tau = 5 \times 10^{-3}$, and $N = 40$. The number of MC blocks was $\sim O(10^3)$, similarly for the number of MC steps for each block.

In order to compute the local SFFs in the individual CHOCL wells using Eq.(36), we divided the large volume of our cubic OL into 27 smaller cubic cells of equal sizes d^3 . The cube edge was equal to the lattice spacing $d = \pi/k$. The central cell was centered at the origin (000) with its faces parallel to the coordinate planes, the rest of the cells being centered at the other lattice sites. By restricting Eq.(36) to the boundaries of each cell volume, we were able to compute the SFF $(\rho_s/\rho)_{(ijk)}$ in each lattice well. For each cell (ijk) , we compute $(\rho_s/\rho)_{s(ijk)}$ using only the particles which are positioned inside the cell according to the boundary conditions

$$\mathbf{r} \equiv \begin{cases} x & : \quad \left(i - \frac{1}{2}\right) \frac{\pi}{k} < x < \left(i + \frac{1}{2}\right) \frac{\pi}{k}, \\ y & : \quad \left(j - \frac{1}{2}\right) \frac{\pi}{k} < y < \left(j + \frac{1}{2}\right) \frac{\pi}{k}, \\ z & : \quad \left(k - \frac{1}{2}\right) \frac{\pi}{k} < z < \left(k + \frac{1}{2}\right) \frac{\pi}{k}. \end{cases} \quad (37)$$

That is, considering (37) the local SFF is

$$\left(\frac{\rho_s}{\rho}\right)_{(ijk)} = \left(\frac{\rho_s}{\rho}\right) \times \frac{N}{\langle N_{(ijk)} \rangle}. \quad (38)$$

In this paper, $(\rho_s/\rho)_{(ijk)}$ is computed using the latter equation, but sometimes it is found more reasonable to compute it *with respect to the total N* , particularly if $\langle N \rangle_{(ijk)} \rightarrow 0$ in the local MI phase. That is, we use (36) plus (37), but without multiplying by the factor $N/\langle N_{(ijk)} \rangle$.

E. Optical densities

In this article, we are also concerned with the average VPI integrated optical 2D density, $\langle n_{2D}(x, y) \rangle$. The integration is of the total density along the z -axis. That is, we first define a density $n_{2D,c}(x, y)$ for each VPI configuration c such that

$$n_{2D,c}(x, y) = \int_{-\infty}^{+\infty} |\Psi_c(x, y, z)|^2 dz, \quad (39)$$

where $\Psi_c(x, y, z)$ is the wavefunction [Eq.(4)] obtained for a certain VPI configuration c . Then one takes the average over all P configurations

$$\langle n_{2D}(x, y) \rangle = \frac{1}{P} \sum_{c=1}^P n_{2D,c}(x, y). \quad (40)$$

Next to this, we also display at some point the 1D optical density, $\langle n_{1D}(x) \rangle$, which is obtained by integrating the 2D density along one of the axes:

$$\langle n_{1D}(x) \rangle = \int_{-\infty}^{+\infty} dy \langle n_{2D}(x, y) \rangle. \quad (41)$$

We therefore would like to point out, that in Ref.[39] we mistakenly wrote that $n_{1D}(x) = \langle n_{2D}(x, y = 0) \rangle$, whereas it should be as in Eq.(41). Nevertheless, in the main text of Ref.[39] and in its figure captions, it was clearly indicated that $n_{1D}(x)$ is the integrated 1D optical density, i.e., as in Eq.(41) above.

F. Units

As in Ref.[39] we use units of the trap, $a_{ho} = \sqrt{\hbar/(m\omega_{ho})}$ and $\hbar\omega_{ho}$ for lengths and energies, respectively, all throughout our calculations. That is, $\mathbf{r} \rightarrow \mathbf{r}/a_{ho}$, $V_0 \rightarrow V_0/(\hbar\omega_{ho})$, $a_c \rightarrow a_c/a_{ho}$, $V_{ho}(\mathbf{r}) \rightarrow V_{ho}(\mathbf{r})/(\hbar\omega_{ho}) = (1/2)r^2$, $\mathbf{k} \rightarrow \mathbf{k}a_{ho}$. The optical densities $\langle n_{2D}(x, y) \rangle$ and $\langle n_{1D}(x) \rangle$ are in units of a_{ho}^{-2} and a_{ho}^{-1} , respectively.

III. RESULTS AND DISCUSSION

In this section, we present the results of our numerical calculations. The same systems are considered as in Ref. [39]. The latter are N HC bosons confined inside a cubic OL of $N_L = 3 \times 3 \times 3$ lattice sites plus an external harmonic trap. For further details about the system and the computational setup, please refer to the previous publication [39].

We explore BEC and superfluidity both from a global and a local perspective. The local perspective, pertains

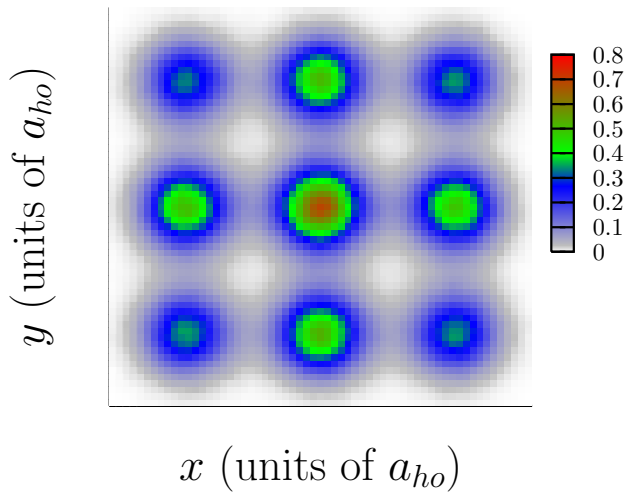


FIG. 1: Density map for a system of $N = 8$ bosons, $V_0 = 10$, and $k = 1.0\pi$ in the same confining geometry as Fig. 3 below. This map is obtained by integrating the three-dimensional density along the z -axis.

to their fractions in each lattice well (or cell), and the global one pertains to these fractions for the whole system (all lattice wells).

From the local perspective, we begin with a brief investigation of the ideal Bose gas, in which we show that the lattice wells have a low CF for $N = 8$ particles when viewed with respect to the global N . Next, we demonstrate the dependence of the CFs $n_{(ijk)}$ and $\tilde{n}_{(ijk)}$ on the HC diameter a_c , where an important role for the interference between the lattice wells is revealed. Similarly, the global and local SFFs, ρ_s/ρ and $(\rho_s/\rho)_{(ijk)}$, respectively, are explored as functions of a_c .

From a global perspective, we chiefly find a counter-intuitive, opposing behavior for the global CF and SFF as functions of $k = \pi/d$. Peculiarly, the SFF drops with increasing k while the CF rises. Additionally, we seek a MI state by going to larger interactions or OL depth, and show that our systems display a coexistence of SF and vacuum MI regimes.

Finally, we also present results for the momentum distributions for some of our systems. The latter reveal a diffractive structure which persists deep into the MI regime [46] suggesting that superfluidity [46] in a CHOCL is found even in the extremely repulsive regime.

A. Numerics

For the CFs at the lattice sites (ijk) , the configurations of previous VMC simulations are used [39]. The local CF is computed as in Sec.IIB, whereas the global one by the additional Eq.(32). The global SFF is computed using Eq.(36) and the local SFF by an additional application of the boundary conditions (37). We use $N = 8$ particles with $V_0 = 10$, and $N = 40$ with $V_0 = 10$ and

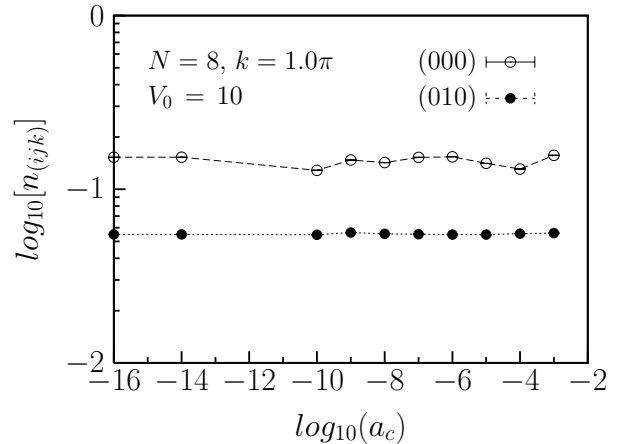


FIG. 2: CF $n_{(ijk)} = N_{(ijk)}/N$ at the central cell (open circles) and (010) (solid circles) as a function of a_c in the extremely dilute regime. The system is a HC Bose gas of $N = 8$ particles, $V_0 = 10$, and $k = 1.0\pi$ in the same confining geometry as Fig. 3 below. A log-log scale is used in order to provide a clearer view of the details. The a_c , k and V_0 are in units of a_{ho} , a_{ho}^{-1} and $\hbar\omega_{ho}$, respectively, where $a_{ho} = \sqrt{\hbar/(m\omega_{ho})}$.

once with $V_0 = 20$. The total number of VPI time slices used is $M = 120$ with a time step $\tau \sim O(10^{-3})$. The number of MC steps and MC blocks is $\sim O(10^3)$.

In order to justify the method outlined in Sec.II, necessitating the presence of spherically symmetric clouds centered at each lattice site, we present in Fig. 1 a map for the integrated VMC density along the z -axis $\langle n_{2D}(x, y) \rangle$ for the system of Fig. 3 below. One can see clearly that the distributions of the atoms about the lattice sites are spherical at the edges of the trap. Thus it can be safely stated, that for a few bosons spherical symmetry is displayed by the lattice clouds, in spite of the presence of an external harmonic trap. Yet by increasing the number of particles, it is anticipated that the clouds at the edges of the trap will be deformed from their spherically symmetric form, as the atoms are pushed away from the trap center towards the edges of the trap by their mutual HC repulsion. This is especially the case, when a_c becomes large. Consequently, in the absence of spherical symmetry, the method of Sec.II cannot be used anymore, except for the clouds which may nevertheless preserve their spherical form. If one uses a large CHOCL with, say, $N_L = 5 \times 5 \times 5$ lattice sites, one must consider a weaker harmonic trap than the one used here in order to maintain spherically symmetric clouds at the edges of the trap.

B. Condensate fraction and interference effects

In this section, we explore the local and global BEC in our CHOCL systems. Only five lattice sites, (000), (001), (010), (011), and (111), which present the whole

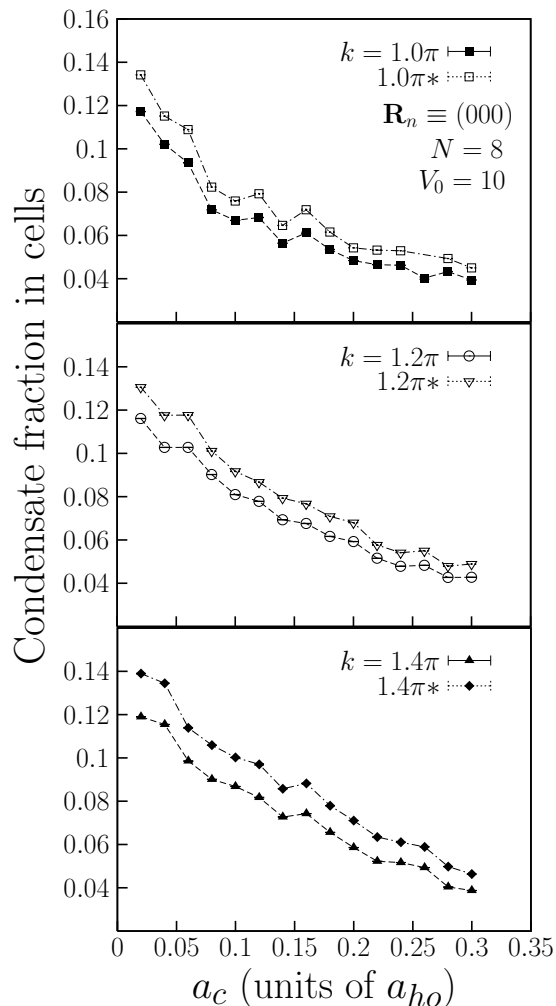


FIG. 3: CFs $n_{(000)}$ and $\tilde{n}_{(000)}$ at lattice site $\mathbf{R}_n \equiv (000)$ versus the HC diameter a_c for systems with and without interference effects, respectively, and at the various k -values indicated. The systems are the same as in Ref.[39]: $N = 8$ HC bosons confined in a cubic OL of $N_L = 3 \times 3 \times 3$ lattice sites plus external harmonic confinement. The height of the OL barrier is $V_0 = 10$. The $\tilde{n}_{(000)}$ values are labelled by (*) in each legend. Solid squares: $k = 1.0\pi$; open squares $k = 1.0\pi^*$; open circles: 1.2π ; open triangles $1.2\pi^*$; solid triangles: 1.4π ; diamonds $1.4\pi^*$. The k and V_0 are in units of a_{ho}^{-1} and $\hbar\omega_{ho}$, where $a_{ho} = \sqrt{\hbar/(m\omega_{ho})}$.

CHOCL system are considered. The role of interference between the lattice wells is revealed by a comparison between $n_{(ijk)}$ and $\tilde{n}_{(ijk)}$.

1. Local CF in ideal BEC

We begin with an investigation of the ideal Bose gas for a_c values ranging from 10^{-16} to 10^{-3} and show that in this regime the local CF is almost stable. The a_c values range from an extremely dilute to dilute regime. Fig. 2 displays the local CF at the central cell (open red circles)

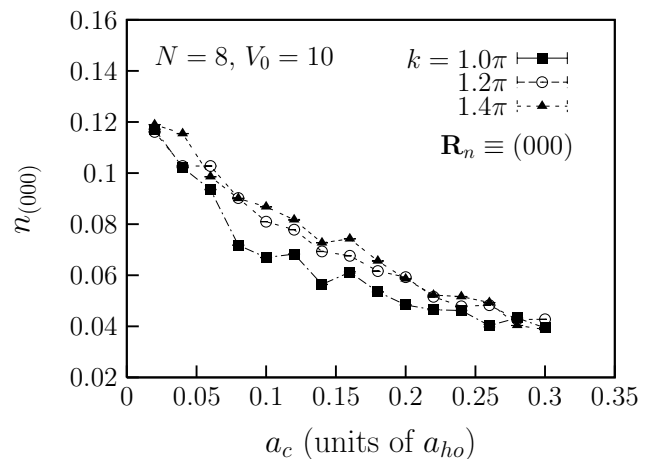


FIG. 4: Same systems as in Fig. 3; but without interference data. The k and V_0 are in units of a_{ho}^{-1} and $\hbar\omega_{ho}$, respectively.

and (010) (solid blue circles). We get $n_{(000)} \sim 15\%$ and $n_{(010)} \sim 5.5\%$ of the total N , which in themselves are small CFs. It should be emphasized that the optimized VMC parameters of the trial wave function (4) are exactly the same for all a_c in the dilute regime. This is because in the dilute regime, the wave function of the system [Eq.(4)] is essentially a product of the Wannier sums Eq.(6) with little effect coming from the Jastrow function.

2. Local CF in the interacting BEC

Fig. 3 displays the CFs $n_{(000)}$ and $\tilde{n}_{(000)}$ (starry labels) in the central well $\mathbf{R}_n \equiv (000)$ versus a_c at the indicated values of k . From the top frame to the bottom frame we display for $n_{(000)}$: (solid squares) $k = 1.0\pi$; (open circles) 1.2π ; (solid up triangles) 1.4π . The systems are the same as in Ref.[39]. For $\tilde{n}_{(000)}$ we display: (open squares) $k = 1.0\pi^*$, (open down triangles) $1.2\pi^*$, and (diamonds) $1.4\pi^*$. Fig. 4 is the same as Fig. 3, but without interference data. The goal of Fig. 4 is to give further manifestation to the dependence of $n_{(000)}$ on k . One can see that for all values of k in the latter figures, $n_{(000)}$ and $\tilde{n}_{(000)}$ decrease with an increase in a_c . Further, the $\tilde{n}_{(000)}$ lies higher than $n_{(000)}$ for all k , indicating that interference between the lattice wells boosts the CF in each well. In Fig. 4, the values of $n_{(000)}$ seem to rise with increasing k in the range $0.05 \leq a_c \leq 0.25$, although for $k = 1.2\pi$ and 1.4π the values are very close to each other.

Fig. 5 is the same as Fig. 3, but for $\mathbf{R}_n \equiv (001)$, (010), (011), and (111), ordered respectively from the top frame to the bottom frame. The same labels are used as in Fig. 3. However, whereas n and \tilde{n} decrease with increasing a_c for (001) and (010), they surprisingly increase for (111) and (011). Some condensate has tunneled away from the sites $\mathbf{R}_n \equiv (000)$, (001), and (010) towards (011) and (111) as a result of an increase in the mutual repulsion

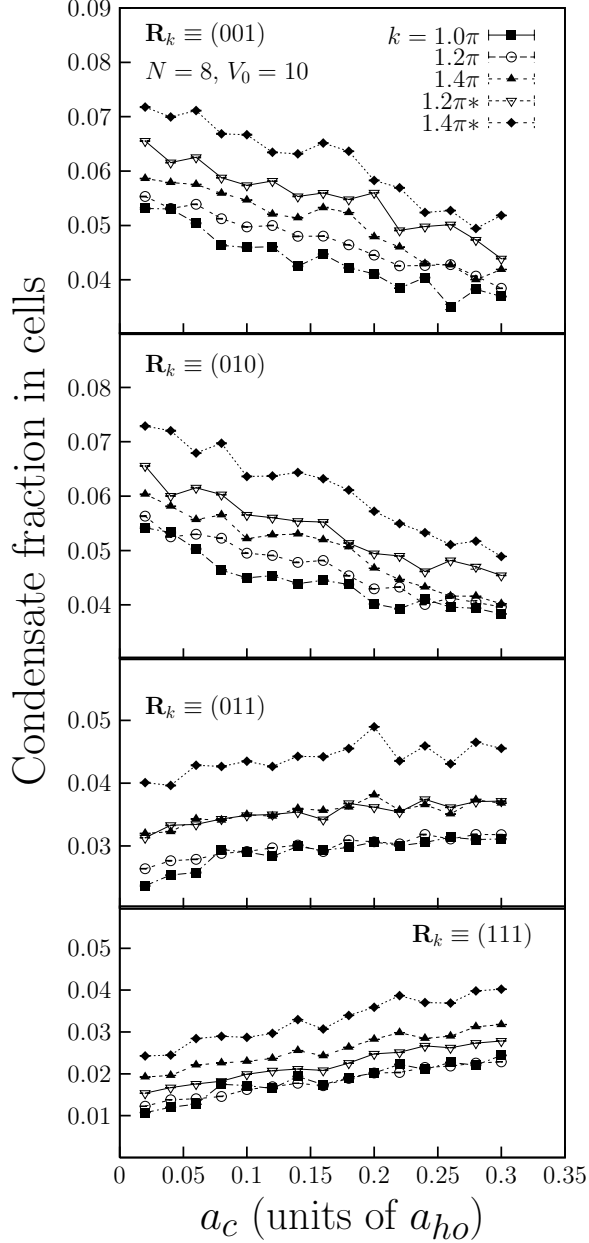


FIG. 5: As in Fig. 3; but from top to bottom for lattice sites $\mathbf{R}_n \equiv (001)$, (010) , (011) , and (111) . The k and V_0 are in units of a_{ho}^{-1} and $\hbar\omega_{ho}$, where $a_{ho} = \sqrt{\hbar/(m\omega_{ho})}$.

of the bosons which drives them away from the center of the trap. A similar expulsion of the BEC towards the edges of the trap has also been encountered in the simple harmonic trap without an OL [40, 47]. This phenomenon corresponds also to a rise in the occupancy of the lattice wells at the corners of the CHOCL with increasing a_c , as demonstrated in Sec.III E later on. Otherwise, Fig. 5 displays the same features as Fig. 3 regarding the values of k and the interference effects. The rise of $n_{(ijk)}$ with increasing k is even more pronounced in Fig. 5. One can explain this by approximating each lattice well by a HO

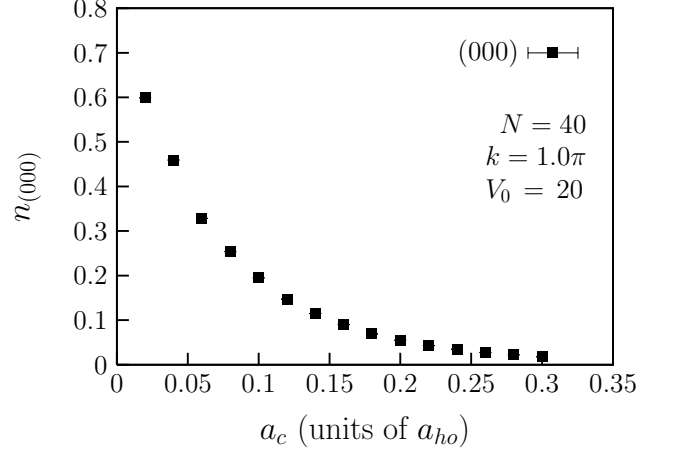


FIG. 6: CF $n_{(000)}$ versus the HC diameter a_c for a system of $N = 40$, $V_0 = 20$, and $k = 1.0\pi$ in the same trapping geometry of Fig. 3. The k and V_0 are in units of a_{ho}^{-1} and $\hbar\omega_{ho}$, respectively, where $a_{ho} = \sqrt{\hbar/(m\omega_{ho})}$.

trap, whose trapping frequency ω_k rises with increasing lattice wave vector $k = \pi/d$. As a result of increasing ω_k , the level spacing $\sim \hbar\omega_k$ becomes larger, thus increasing the energy needed to excite atoms out of the ground state HO level. Consequently, more particles find themselves forced to condense into the lowest “harmonic oscillator” level. (We did not include in Fig. 5 \tilde{n} for $k = 1.0\pi^*$ in order not to clutter the figures.)

Another explanation is as follows. Going back to Fig. 15 of Ref.[39], one can see that the occupancy of the central well (000) and the first neighbor (00 -1) decreases with increasing k . [Note that (00 -1) belongs to the same lattice site family of (010) and (001).] Consequently, the reduction in the occupancy reduces the density in these lattice wells, and henceforth the onsite interactions between the bosons. This in turn reduces the depletion effect of the HCs causing a rise in the CFs with increasing k as observed in Figs. 3–5. It is further noted that $n_{(001)}$ is changing with a_c at a lower rate than $n_{(000)}$. E.g, $n_{(001)}$ for $k = 1.0\pi$ (solid squares) in Fig. 5 declines from ~ 0.055 down to ~ 0.04 over the whole range of a_c in the figure, whereas $n_{(000)}$ for the same k (see Fig. 4) decreases from ~ 0.12 to ~ 0.04 . The same feature is observed for $\mathbf{R}_n \equiv (010)$ when compared to (000). In contrast, $n_{(111)}$ and $n_{(011)}$ increase by ~ 0.01 in Fig. 5. Hence, the rate of change of the $n_{(ijk)}$ with a_c , whether $n_{(ijk)}$ is rising or declining, becomes smaller as the lattice well approaches the edges of the trap. This is attributed to the fact that the energy cost required for the bosons to tunnel through (or between) two neighboring CHOCL wells increases as the lattice wells approach the edges of the background harmonic trap. This is because each lattice well is superimposed on the harmonic trap. Therefore the potential energy minimum of each lattice well at position \mathbf{R}_n from the trap center, is equal to the HO energy $(1/2)|\mathbf{R}_n|^2$ and rises with increasing $|\mathbf{R}_n|$. In addition, we present

in Fig. 6 the behavior of the CF $n_{(000)}$ for $N = 40$ particles, $V_0 = 20$, and $k = \pi$. Again, the BEC gets depleted with increasing a_c , except that the CFs are substantially higher than for $N = 8$.

It must be emphasized, that the values of the CFs in Figs. 3–5 fluctuate with a_c due to the small number of particles, $N = 8$, used which causes real physical fluctuations to be large [48]. Nevertheless, the trend in the CFs clearly indicates depletion with increasing a_c for some lattice cells and a condensate buildup in other cells. It is further noted, that in general the CFs for $N = 8$ are significantly lower than 1, bringing this result in line with the earlier findings of Sun *et al.* [3]. For $N = 40$, the data varies smoothly with a_c and the statistics are good, demonstrating that a higher N leads to lower condensate number fluctuations inside the OL.

3. Global CF n_0

Using the previous results of Figs. 3– 5 for the non-interfering case only, we can estimate the global CF n_0 using Eq.(32). The goal is to distinguish between condensate local and global behavior. Fig. 7 displays n_0 for the systems in the latter figures at $k = 1.0\pi$ (solid squares), 1.2π (open circles), and 1.4π (solid triangles). It is noted, that n_0 is practically constant and not sensitive to the changes in the repulsive forces via a_c . This is a peculiar result, suggesting that the CF is globally conserved. In contrast, the decline of $n_{(ijk)}$ with increasing a_c at the lattice sites (000), (001), and (010) in Figs. 3– 5 is a local effect and was compensated by a corresponding rise at (011) and (111). The n_0 for $k = 1.0\pi$ is $\sim 80\%$ for all values of a_c , whereas for $k = 1.2\pi$ and 1.4π , $n_0 \sim 85\%$ and $\sim 100\%$, respectively, for all a_c . The values of n_0 are high because for $N = 8$ particles the systems are in the dilute

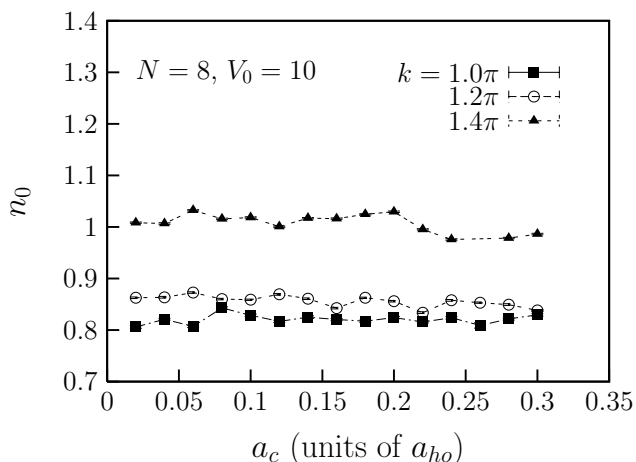


FIG. 7: Global CF n_0 as estimated by Eq.(32) for the systems in Fig. 3 at $k = 1.0\pi$ (solid squares); $k = 1.2\pi$ (open circles), and $k = 1.4\pi$ (solid triangles). The k and V_0 are in units of a_{ho}^{-1} and $\hbar\omega_{ho}$, respectively, where $a_{ho} = \sqrt{\hbar/(m\omega_{ho})}$

regime and remain in this state even up to very large HC repulsion. Further, the global CF is boosted with the rise of k (the local-confinement strength $\omega_k \propto k = \pi/d$) in each CHOCL well. The OL introduces a local depletion effect at lower $k < 1.4\pi$ when there is almost no role for the HC repulsion in the global depletion. An important finding, then, is that the BEC in a CHOCL with a few bosons is chiefly depleted by the OL. Therefore, whereas the global CF n_0 remains constant as a_c is changed, the local CF is redistributed at the various lattice sites. In contrast, Ramanan *et al.* [33] found that for a 1D Bose gas trapped by an OL plus a weak external harmonic trap, the total CF is depleted substantially with an increase of the onsite repulsive energy U . Using the BHM, van Oosten *et al.* [12] demonstrated that the CF in a 2D and 3D OL decreases with increasing parameter U/t , where U is the contact interactions strength and t the hopping amplitude.

C. Superfluid fraction

In this section, we explore the SFF in our CHOCL systems both as a global and as a local quantity in individual lattice wells. We consider systems with $N = 8$ and $N = 40$ bosons in the same confining geometry as in Fig. 3 with the same k -values and $V_0 = 10$. The SFF is computed globally using Eq.(36), and locally for $a_c \leq 0.3$ by Eq.(38) and an additional application of the boundary conditions (37). For the larger $a_c \sim O(1)$, the SFF was computed with respect to the *total* N as outlined later below. We did not compute the SFF for the systems with $N = 8$ particles for the range of $a_c \leq 0.3$ considered so far because of the high statistical fluctuations in the values of the VPI MC block averages. However, at extreme values of a_c beyond 1.00, these fluctuations are much lower, and therefore it was reasonable to report the SFF for $N = 8$ as in Sec.III E below.

1. Global SFF ρ_s/ρ

Fig. 8 displays the global SFF, ρ_s/ρ , versus a_c for the latter systems at the indicated values of k . The labelling is as in Fig. 7. One can see that the global SF is depleted with a rise in a_c . Further, the values of ρ_s/ρ decrease with increasing k , and one can conclude that a higher k (lower lattice spacing) enhances the depletion of the global SF in an OL. This is our chief result and is counter-intuitive to the rise of the global CF with increasing k as in Fig. 7. Retrospectively, this could also be explained as before [39]: a smaller lattice spacing increases the localization of the bosons inside each lattice cell and causes a reduction in their superflow. A reduction in superflow means a smaller number of particles possessing enough kinetic energy for tunneling from one well to another. Further note that remarkably even at very strong repulsion between the bosons, superfluidity

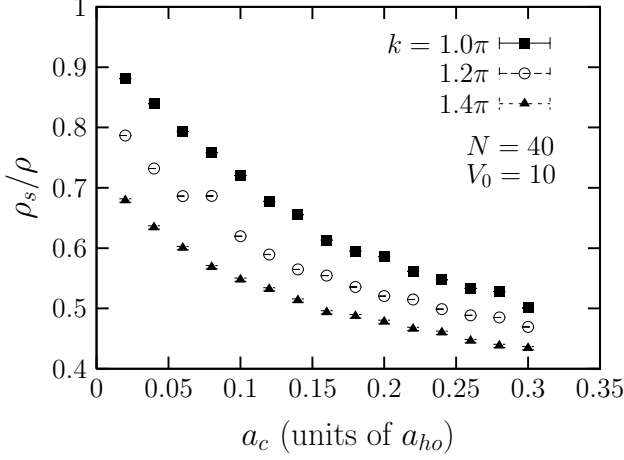


FIG. 8: Global SFF ρ_s/ρ versus the HC diameter a_c as computed by the diffusion formula of Pollock and Ceperely [41] given here by Eq.(36). The system considered is $N = 40$ HC bosons in the same trapping geometry of Fig.3 and the indicated values of k . The same labels are used as in Fig. 5. The k and V_0 are in units of a_{ho}^{-1} and $\hbar\omega_{ho}$, respectively, where $a_{ho} = \sqrt{\hbar/(m\omega_{ho})}$.

is still present ($\rho_s/\rho \gtrsim 40\%$ for $a_c = 0.3$.) In contrast to the global BEC in Fig. 7, a_c plays a chief role in the global depletion of the SF in Fig. 8.

2. Local SFF $(\rho_s/\rho)_{(ijk)}$

As for the SFF in each CHOCL cell, $(\rho_s/\rho)_{(ijk)}$, it reveals a different behavior as compared to its global character in Fig. 8. Fig. 9 displays $(\rho_s/\rho)_{(ijk)}$ vs. a_c for the same systems of Fig. 8, where for the top frame to the bottom frame: $k = 1.0\pi$, 1.2π , and 1.4π , respectively. Solid squares: $(ijk) \equiv (000)$; open circles: (010) ; solid circles: (011) ; open triangles: (111) . Inside each cell, the local $(\rho_s/\rho)_{(ijk)}$ is computed using Eq.(38) plus the condition (37).

The same features are observed in all three frames: $(\rho_s/\rho)_{(011)}$ and $(\rho_s/\rho)_{(111)}$ rise with increasing a_c . The $(\rho_s/\rho)_{(010)}$ displays an initial weak decline, but then it stabilizes somewhat after $a_c = 0.2$. For the center (000) the decline is more pronounced than in (010) up to $a_c = 0.16$, after which it stabilizes somewhat. In fact, the rise of $(\rho_s/\rho)_{(011)}$ and $(\rho_s/\rho)_{(111)}$ with increasing a_c conforms to the rise of the CFs $n_{(011)}$ and $n_{(111)}$ with a_c in Fig. 5 (although for a different number of particles), whereas the decline in (000) corresponds to that of $n_{(000)}$ in Fig. 4. It can therefore be argued, that locally the behavior of the SF is isomorphic to that of the condensate. Although N is different, it is important to emphasize that the local SFFs in Fig. 9 are of the same order of magnitude as the local CFs in Fig. 5. The reduction in $(\rho_s/\rho)_{(000)}$ is in line with the previous finding [39], that a rise in a_c reduces the single-particle tunneling ampli-

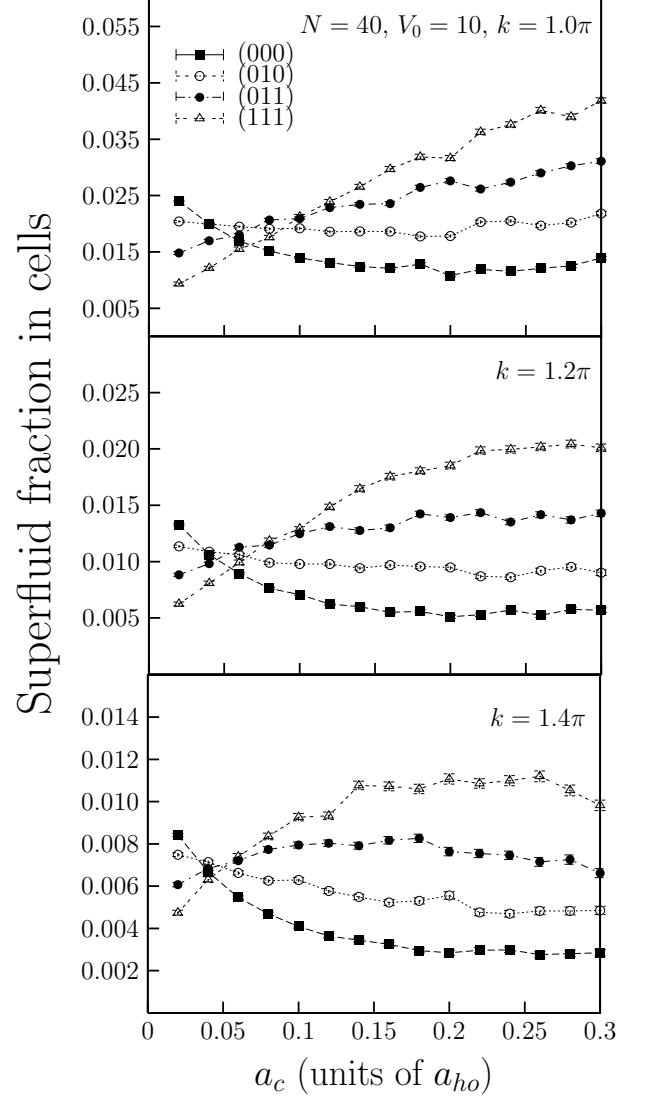


FIG. 9: As in Fig. 8; but for the local SFF $(\rho_s/\rho)_{(ijk)}$ at the indicated values of k . The cell boundaries are given by Eq.(37). The $(\rho_s/\rho)_{(ijk)}$ is computed via Eq.(38) by using the number of particles $N_{(ijk)}$ inside each cell instead of the total number of particles N . Solid squares: $(ijk) \equiv (000)$; open circles: (010) ; solid circles: (011) ; open triangles: (111) . The k and V_0 are in units of a_{ho}^{-1} and $\hbar\omega_{ho}$, respectively, where $a_{ho} = \sqrt{\hbar/(m\omega_{ho})}$.

tude J between, e.g., the central (000) and first neighbor (010) cells. The superflow is therefore suppressed between those lattice wells because of an increased localization at the larger a_c .

By inspecting Fig. 9, one notes again a similar counter-intuitive feature as for the global values; that for each cell the local SFF drops with increasing k contrary to the corresponding local CF in Fig. 5. Another peculiar feature in Fig. 9, is that all four curves in each frame intersect almost at the same value of a_c where there is

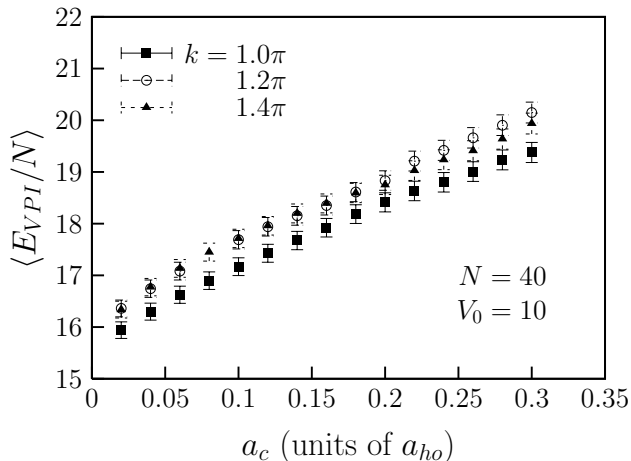


FIG. 10: Average VPI energy per particle, $\langle E_{VPI}/N \rangle$, versus the HC diameter a_c for the same systems of Fig. 8. The k is in units of a_{ho}^{-1} where $a_{ho} = \sqrt{\hbar/(m\omega_{ho})}$. The $\langle E_{VPI}/N \rangle$ and V_0 are in units of $\hbar\omega_{ho}$.

almost an equal distribution of the SF at all lattice sites. The SF migrates from the cells near the center of the trap towards the corners of the CHOCL with the increase of a_c . This feature is also elaborated in Sec.III E below, where systems with extremely repulsive HCs are investigated.

The effects of an external harmonic trap are as such to introduce a new behavior for the superflow of bosons between the wells of an OL. As the repulsive interactions become stronger, the SF is “expelled” towards the edges of the trap analogous to the condensate in a simple harmonic trap [40, 47]. However, in a CHOCL parts of the condensate still remain situated in the lattice wells close to the center of the trap.

D. Energies

Fig. 10 displays the behavior of the average VPI energy per particle, $\langle E_{VPI}/N \rangle$, as a function of the HC diameter a_c for the same systems in Fig. 8. Whereas $\langle E_{VPI}/N \rangle$ rises with increasing a_c , ρ_s/ρ decreases (see Fig. 8). The rise in the energy is chiefly due to the rise in the average onsite interaction energy $\langle U_{(pqr)} \rangle$ with a_c , as found earlier in Ref.[39]. Therefore, the later rise overwhelms the drop in kinetic energy, i.e. mobility, in favor of an increase in boson localization.

E. Can we get a pure Mott insulator?

In this section, we show that for a few bosons in a CHOCL with a limited number of lattice sites, MI regimes can be achieved by increasing the HC diameter of the bosons to large values. It is found that only a part of the system will be in the MI state where a number

of CHOCL wells display the absence of superfluidity. We show that our systems are different than the ones usually treated by the BHM for a much larger number of particles N . For example, Hen and Rigol [13] explored the phase diagram of a HC BHM on a checkerboard superlattice. According to Hen and Rigol [13–15], bosons inside a CHOCL display coexisting SF and MI phases. Mixed SF-MI regimes have also been experimentally reported by Spielman *et al.* [19, 46] in 2D atomic gases confined in harmonic OL potentials. In the work of Jaksch *et al.* [49], a checkerboard SF-MI phase was observed in an OL. Their most important finding was that a BHM could be realized by the dynamics of bosons in an OL. But this was found for a much larger number of particles and lattice sites than ours, using a discrete space approach, whereas our investigation is restricted to a few bosons and lattice sites in continuous space.

Hen and Rigol [15] explored the ground state properties of HC bosons in 2D and 3D OLs confined by an external harmonic trap. It was demonstrated that a MI state usually displays a flat density along several lattice sites, as in their Figs. 7 and 14, where the density is displayed as a function of the distance from the center of the trap. However, a limited number of lattice sites as in the present work here does not furnish the ground for obtaining a flat density profile.

In the investigations of Hen and Rigol [13, 15, 26] and Jaksch *et al.* [49] the interactions are described by contact potentials and have no range (a_c) as in our case. Thus, the BHM cannot be used here to make predictions about a possible SF-MI transition. In fact, a large increase in a_c causes –as shown next– the bosons to be driven out of the center of the trap towards the corners of the CHOCL, instead of making them prefer to occupy sites individually as in the BHM. This is because when the volume of each HS boson is increased, they have no other way but to increase their minimum separation as they are not able to approach each other by a distance less than a_c , prescribed by the Jastrow function (5). Therefore, a homogeneous distribution cannot be achieved. Hence, increasing a_c largely in our systems does not yield a pure MI state throughout the whole lattice wells. We are thus very much inclined to say, given the above information, that our systems will retain an SF even in the strongly interacting regime.

In the BHM, on the other hand, a large increase in the repulsive contact potential makes it energetically more costly to hop from one lattice well to another, but it does not increase the volume of the HS bosons. A homogeneous distribution is thus naturally possible in the BHM as the bosons seek the lowest energetic configuration in the OL.

Further, in contrast to Hen and Rigol [15], the vacuum surrounding our CHOCL does not contain empty lattice sites, and therefore cannot be associated with an empty MI state. The empty MI regime was mentioned earlier [15]. However, inside the CHOCL it will be demonstrated that vacuum MI states are possible.

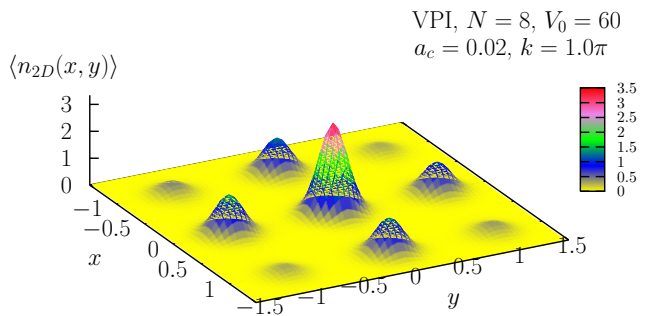


FIG. 11: Integrated VPI density along the z -axis $\langle n_{2D}(x, y) \rangle$ [Eq.(40)] of a system with $N = 8$, $a_c = 0.02$, $k = 1.0\pi$. The trapping geometry is the same as that of the systems in Fig. 3, except that the OL potential barrier is $V_0 = 60$. The a_c , k and V_0 are in units of a_{ho} , a_{ho}^{-1} and $\hbar\omega_{ho}$, respectively, where $a_{ho} = \sqrt{\hbar/(m\omega_{ho})}$. The x and y are in units of a_{ho} , and $\langle n_{2D}(x, y) \rangle$ is in units of a_{ho}^{-2} .

In order to check for the presence of a SF phase in some parts of our systems for large a_c , one could compute $U/(zJ)$ between two neighboring lattice sites. This should help us shed more light on the state of the current CHOCL systems, because it is hard to distinguish between a SF and MI by only looking at the densities. The identification of MI domains only by means of the density was found to be inaccurate, as outlined earlier by Rigol *et al.* [14] (and references therein). Earlier, it was found [39] that for a_c up to 0.3 our systems were still in the SF phase and that $U/(zJ)$ began to stabilize for large a_c . For the tunneling from the central cell (000) to the first nearest neighbor (00 -1), our calculations yielded a $U/(zJ) \ll 5.814$ (see Fig.6 in Ref.[39]). However, for the much larger a_c values used next, an evaluation of $U/(zJ)$ was not possible since a VMC ground-state wave function was not obtainable anymore for $a_c \geq 1$. This is because VMC reweighting [40] breaks down at these large interactions. Instead, we resorted to evaluate the VPI SF fraction in each lattice well as was done in Sec.III C.

1. Large V_0

First, we tried to obtain a *pure* MI by an increase of V_0 . In Fig. 11, we show such a case of high V_0 . There, we display the integrated VPI density $\langle n_{2D}(x, y) \rangle$ [Eq.(40)] for a system of $N = 8$, $V_0 = 60$, $a_c = 0.02$, and $k = 1.0\pi$ in the same trapping geometry as that of the systems of Fig. 3. The corresponding Fig. 12 displays the integrated 1D VPI density $\langle n_{1D}(x) \rangle$ (open circles), Eq.(41) of Fig. 11 along the x -axis. The solid line is the integrated 1D VMC density obtained by Eq.(41) as for VPI. It is a VMC best “fit” to the VPI data, obtained by manually fitting the parameters of the 3D VMC trial function [Eq.(4)] to the 1D VPI density. The goal was to use the “fitted” VMC trial function to compute the ratio $\langle U_{(000)} \rangle / [6 \langle J_{(000) \rightarrow (100)} \rangle]$ [39] between the central cell

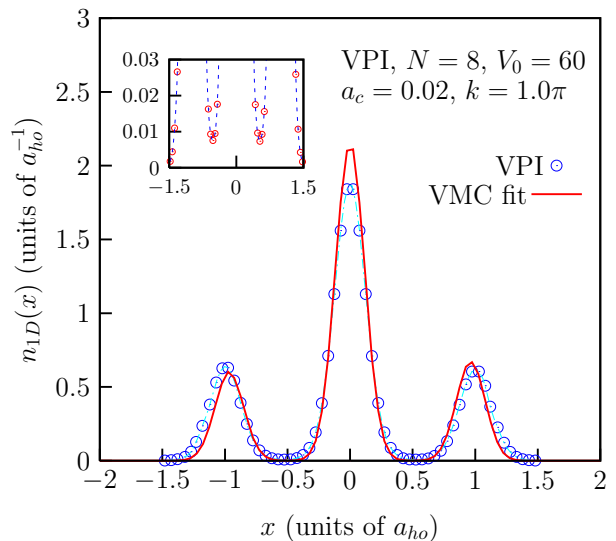


FIG. 12: Integrated VPI 1D optical density $\langle n_{1D}(x) \rangle$ [Eq.(41)] of Fig. 11 (open circles) along the x -axis. The solid red line is a VMC best “fit” to the VPI data using the trial wave function Eq.(4). The inset is the same figure; but taken for a much smaller density range in order to reveal the overlap of the wave function between the lattice sites. The a_c , k and V_0 are in units of a_{ho} , a_{ho}^{-1} and $\hbar\omega_{ho}$, respectively, where $a_{ho} = \sqrt{\hbar/(m\omega_{ho})}$.

and a first neighbor cell in order to make a decision about the state of the system. It was found that the latter ratio equals 0.015 which is much less than 5.8, placing the system of Fig.12 in the SF regime. We must also emphasize that the above ratio is difficult to obtain using VPI, as this method does not optimize a parameterized trial function, but is rather independent of a trial function. Next to this, the VMC method failed to “automatically” optimize the trial wave function at this high value of V_0 in order to reach a ground-state. This is the reason why we resorted to a “manual” optimization.

The upper left inset of Fig. 12 shows a magnified view of the VPI density-overlap between the lattice wells. In Fig. 11, one can see that the tunneling of the BEC between the lattice wells is substantially reduced, however, upon a careful inspection of Fig. 12 and the inset, one can see that some overlap remains between the lattice wells. In fact, Eq.(36) reveals a global SFF of $(23.93 \pm 0.06)\%$ for that system. That is, superfluidity is still present at this high V_0 .

2. Large a_c

Second, we tried to obtain a pure MI by increasing a_c substantially. Therefore, Fig. 13, displays several densities $\langle n_{2D}(x, y) \rangle$ for the same system of Fig. 3 with $k = 1.0\pi$, obtained by increasing a_c to extreme values: $a_c = 1.00$ [frame (a)]; 1.10 [frame (b)]; 1.50 [frame (c)];

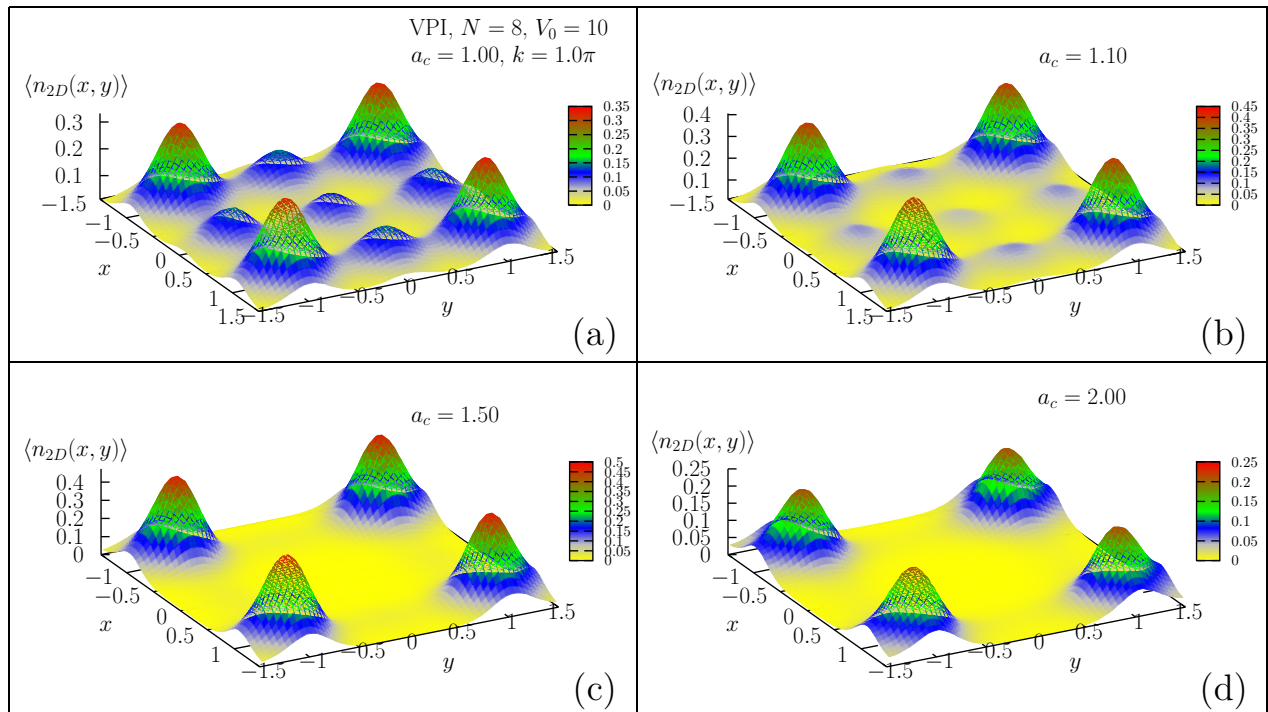


FIG. 13: As in Fig. 11; but for $V_0 = 10$ and (a) $a_c = 1.00$, (b) 1.10 , (c) 1.50 , and (d) 2.00 , respectively. The a_c , k and V_0 are in units of a_{ho} , a_{ho}^{-1} and $\hbar\omega_{ho}$, respectively, where $a_{ho} = \sqrt{\hbar/(m\omega_{ho})}$. The x and y are in units of a_{ho} , and $\langle n_{2D}(x, y) \rangle$ is in units of a_{ho}^{-2} .

and 2.00 [frame (d)], respectively. The density-peaks at the corners of the CHOCL have the largest amplitudes as the particles are repelled away from the center of the trap. At this a_c , the particles prefer to occupy the corners to reduce the repulsive potential energy, but in (a) and (b) there is still some small probability for them to occupy the wells closer to the center of the trap. It turns out that for (a) and (b) there remains BEC overlap (tunneling) between the lattice wells and their global SFF is $(46.31 \pm 0.07)\%$ for $a_c = 1.00$ and $(39.82 \pm 0.31)\%$ for $a_c = 1.10$. The $\langle n_{1D}(x) \rangle$ of Fig. 13(a) displayed in Fig. 14 reveals a remaining BEC overlap between the wells signalling the presence of superfluidity. For even larger a_c , notice that the central wells are almost vacant in both frames (c) and (d) of Fig. 13, as the extremely strong repulsion has expelled all the atoms from the central cells. However, upon inspecting the $\langle n_{1D}(x) \rangle$ in Fig. 15 corresponding to Fig. 13(d), one can observe for $a_c = 2.00$ a still-existing BEC overlap between the lattice wells via the central cell, with a global SFF of $(22.46 \pm 0.05)\%$.

To this end, the main question that remains, then, is whether our systems above are only an SF, or a mixture of coexisting SF and MI regimes. One can possibly answer this question by computing the occupancies $\langle N_{(ijk)} \rangle$ of the individual lattice wells [50], using the counting method in Ref.[39]. If $\langle N_{(ijk)} \rangle$ is an integer, then one can talk about a MI. In that sense, Table I presents $\langle N_{(ijk)} \rangle$ obtained by VPI for the densities in Figs. 11 and

13(a)–(d). In general, the $\langle N_{(ijk)} \rangle$ are all fractions and not integers, and $\langle N_{(000)} \rangle$, $\langle N_{(010)} \rangle$, and $\langle N_{(011)} \rangle \rightarrow 0$ for $a_c = 1.50$ and 2.00 , respectively. It might then be possible to argue that the empty cells in Figs.13(c) and (d) could constitute a empty (vacuum) MI regime. Therefore the CHOCL systems always retain a SF component coexistent with MI regimes.

For a decisive check of the latter possibility, the local SFF *with respect to the total N*, i.e. Eq.(36) plus the condition (37), was computed for the same systems of Fig. 13 at $a_c = 1.50$ and 2.00 . The reason for taking the SFF with respect to N instead of $\langle N_{(ijk)} \rangle$, is because the wells (000) , (010) , and (011) have a very low occupancy $\langle N_{(ijk)} \rangle$ for $a_c > 1.20$; they are close to being empty. Therefore, it does not make sense to compute the SFF with respect to $\langle N_{(ijk)} \rangle$ as we did for the lower a_c in Sec.III C 2.

Table II presents results for $a_c > 1.2$ and the same lattice wells as in Table I. Viewed from this angle, the SFF is negligibly small in all lattice wells. There is a nonsignificant SFF of $\sim 1\%$ for the well (111) at $a_c = 1.50$, indicating that some SF has migrated to the corners of the CHOCL. The lattice wells with a negligible SFF define a local MI phase. In contrast, the global SFF is significant.

TABLE I: VPI occupancies $\langle N_{(ijk)} \rangle$ of the systems in Figs. 11 and Figs. 13(a-d), plus an additional system at $a_c = 1.20$ (density not shown), at various lattice sites (cells) $\mathbf{R}_n \equiv (ijk)$ representative of the whole OL. From left to right: a_c is the HC diameter, V_0 is the OL depth, followed by the cells (000), (010), (011), and (111), respectively. Lengths and energies are in trap units $a_{ho} = \sqrt{\hbar/(m\omega_{ho})}$ and $\hbar\omega_{ho}$, respectively.

| a_c | V_0 | (000) | (010) | (011) | (111) |
|------------|----------------------|--|--|--|-------------------------------------|
| (a_{ho}) | $(\hbar\omega_{ho})$ | | | | |
| 0.02 | 60 | 1.382 $\pm 3.169 \times 10^{-3}$ | 0.536 $\pm 2.449 \times 10^{-3}$ | 0.222 $\pm 1.797 \times 10^{-3}$ | 0.058 $\pm 9.103 \times 10^{-4}$ |
| 1.00 | 10 | 0.134 $\pm 1.338 \times 10^{-3}$ | 0.125 $\pm 1.101 \times 10^{-3}$ | 0.227 $\pm 1.446 \times 10^{-3}$ | 0.471 $\pm 1.936 \times 10^{-3}$ |
| 1.10 | 10 | 0.090 $\pm 1.255 \times 10^{-3}$ | 0.075 $\pm 8.760 \times 10^{-4}$ | 0.167 $\pm 1.270 \times 10^{-3}$ | 0.597 $\pm 1.885 \times 10^{-3}$ |
| 1.20 | 10 | 0.015 $\pm 3.723 \times 10^{-4}$ | 0.016 $\pm 2.732 \times 10^{-4}$ | 0.064 $\pm 5.350 \times 10^{-4}$ | 0.787 $\pm 9.054 \times 10^{-4}$ |
| 1.50 | 10 | 6.429×10^{-4} $\pm 7.495 \times 10^{-5}$ | 2.063×10^{-3} $\pm 8.418 \times 10^{-5}$ | 0.027 $\pm 4.349 \times 10^{-4}$ | 0.837 $\pm 9.144 \times 10^{-4}$ |
| 2.00 | 10 | 1.386×10^{-6} $\pm 6.864 \times 10^{-7}$ | 7.444×10^{-5} $\pm 2.485 \times 10^{-5}$ | 5.472×10^{-3} $\pm 1.585 \times 10^{-4}$ | 0.583 $\pm 1.471 \times 10^{-3}$ |

TABLE II: VPI Superfluid fractions (ρ_s/ρ) in individual cells [i.e., with respect to the *total* N using Eq.(36) plus the condition (37)] for some of the same systems in Table I. Lengths and energies are in trap units $a_{ho} = \sqrt{\hbar/(m\omega_{ho})}$ and $\hbar\omega_{ho}$, respectively.

| a_c | V_0 | (000) | (010) | (011) | (111) |
|------------|-----------------|----------------------|--|--|--|
| (a_{ho}) | $(\hbar\omega)$ | | | | |
| 1.50 | 10 | 0.000 ± 0.000 | 6.677×10^{-8} $\pm 2.380 \times 10^{-8}$ | 1.728×10^{-5} $\pm 1.215 \times 10^{-6}$ | 1.067×10^{-2} $\pm 1.742 \times 10^{-5}$ |
| 2.00 | | 0.000 ± 0.000 | 2.005×10^{-7} $\pm 1.610 \times 10^{-7}$ | 4.820×10^{-7} $\pm 1.520 \times 10^{-7}$ | 4.878×10^{-3} $\pm 2.078 \times 10^{-5}$ |

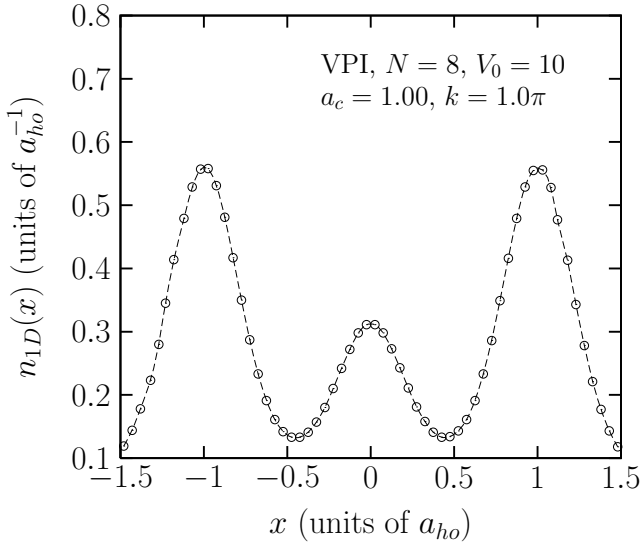


FIG. 14: Integrated VPI 1D optical density $\langle n_{1D}(x) \rangle$ [Eq.(41)] of Fig. 13(a) along the x -axis. The a_c , k and V_0 are in units of a_{ho} , a_{ho}^{-1} and $\hbar\omega_{ho}$, respectively, where $a_{ho} = \sqrt{\hbar/(m\omega_{ho})}$.

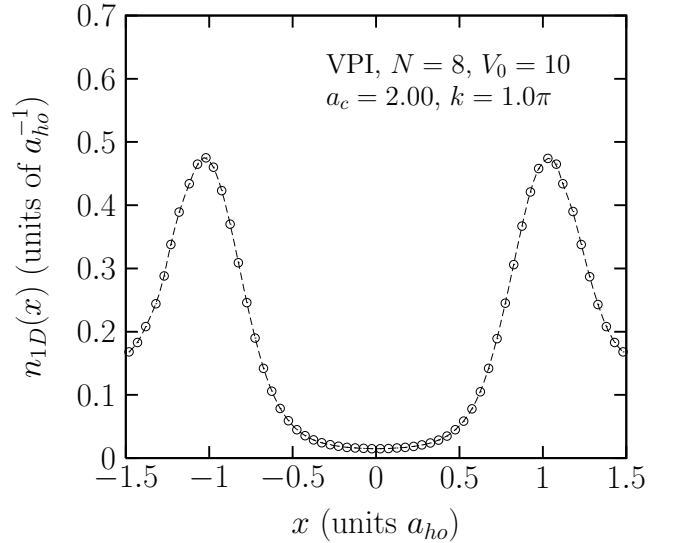


FIG. 15: Integrated VPI 1D optical density $\langle n_{1D}(x) \rangle$ [Eq.(41)] of Fig. 13(d) along the x -axis. The a_c , k and V_0 are in units of a_{ho} , a_{ho}^{-1} and $\hbar\omega_{ho}$, respectively, where $a_{ho} = \sqrt{\hbar/(m\omega_{ho})}$.

In conclusion, the HC Bose gases in the CHOCL traps presented here develop coexisting SF-MI phases at extremely large HS radii a_c . It also turns out, that one must carefully distinguish between global and local superfluidity when it comes to defining local MI domains. The presence of a global SF does not imply the absence of a local MI phase. The systems presented here display a significant global SFF up to $a_c = 2.00$; but the same cannot be stated about the local SFF in the lattice wells.

F. Momentum density

In this section, we conclude with a computation of the k -space momentum distributions of ground-state densities. The goal is to check for the presence of momentum states higher than $k = 0$. According to a discussion by Mullin [51], Chester [52, 53] proved that there can be no BEC in $k > 0$ states unless there is condensation into the $k = 0$ momentum state.

The momentum density is calculated by a numerical Fourier transform (FT) of the spatial density according to

$$\rho_{FT}(k_x, k_y) = \frac{1}{4\pi^2} \int_{-\infty}^{+\infty} dx \int_{-\infty}^{+\infty} dy \langle n_{2D}(x, y) \rangle \exp(-i\mathbf{k} \cdot \mathbf{r}), \quad (42)$$

where $\mathbf{r} = x\mathbf{i} + y\mathbf{j}$, and $\mathbf{k} = k_x\mathbf{i} + k_y\mathbf{j}$, where \mathbf{i} and \mathbf{j} are unit vectors. Fig. 16 reveals $\rho_{FT}(k_x, k_y)$ from the top frame to the bottom frame, respectively for Figs. 11, and 13(a) and (d). One observes that there is always a broad central BEC peak surrounded by Bragg peaks signalling the presence of $k > 0$ states in the system. This is even the case for the system of Fig.13(d), where no central spatial density peak is present. The ρ_{FT} results are another manifestation of the Chester theorem mentioned above.

Next to this, had there been only one broad zero-momentum peak, this would have indicated the presence of a “pure” MI state [18, 26]. The particles are therefore not locked in their positions as in a MI and rather display a mobility, arising from the hopping from one lattice well to another. Further, as a result of trapping, our central BEC density is not a sharp function of the momentum \mathbf{k} . This is in line with the finding of Hen and Rigol [15], who reported that the $\mathbf{k} = 0$ density peak reveals a smoother dependence on \mathbf{k} in a trapped system than a homogeneous system.

Our momentum distributions in Fig. 16 display similar features to Fig.1(a) of Spielman *et al.* [46]. The diffractive structure is indicative of the presence of a SF state (their Fig.17, top frame). As the system progresses into the MI regime, the diffractive structure weakens (their Fig.17, middle and bottom frames), as the intensity of the peaks declines. Accordingly, our results

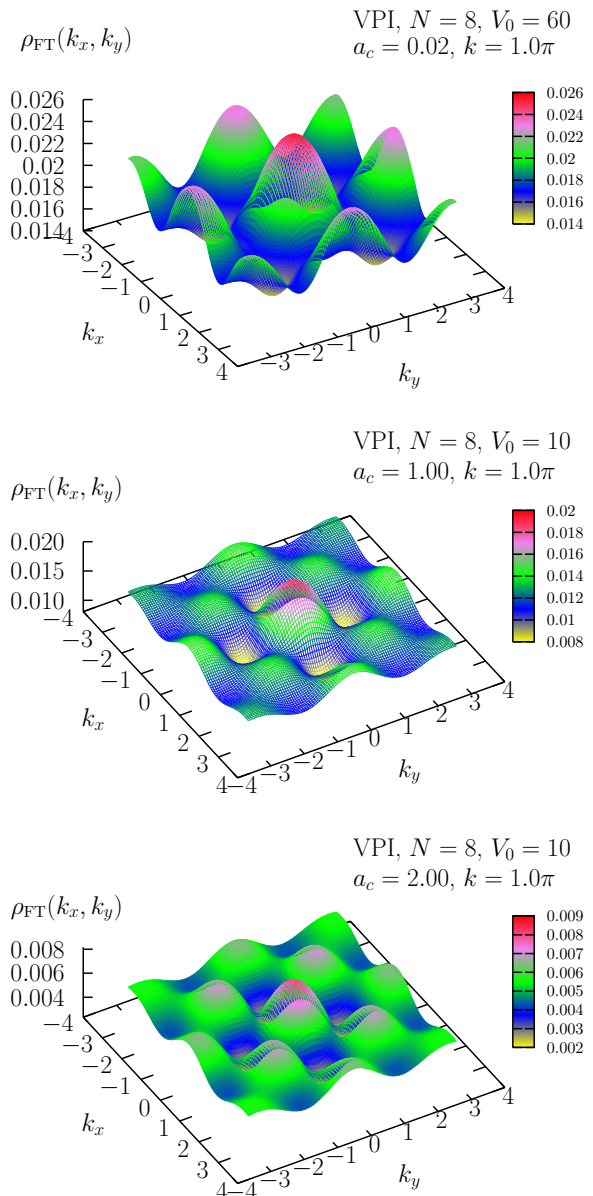


FIG. 16: Momentum densities obtained from Eq.(42). Top frame: $\rho_{FT}(k_x, k_y)$ for Fig. 11; middle frame: for Fig. 13(a); bottom frame: for Fig. 13(d). The $\rho_{FT}(k_x, k_y)$ is in units of a_{ho}^2 , and k_x and k_y are in units of a_{ho}^{-1} , where $a_{ho} = \sqrt{\hbar/(m\omega_{ho})}$. The a_c , k and V_0 are in units of a_{ho} , a_{ho}^{-1} and $\hbar\omega_{ho}$, respectively.

of Fig. 16 are in line with those of Spielman *et al.* [46] who indicated that (citing them:) “the diffractive structure persists deep into the Mott regime”. However, this diffractive structure leads to other manifestations as outlined in the next section. In addition, Gerbier *et al.* [54] experimentally explored phase coherence of ultracold Bose gases trapped in OLs. These authors found that phase coherence persisted in the MI phase by studying the interference pattern of the density distribution of an

expanding ^{87}Rb BEC released from an OL. The persistence of this interference in the MI phase was attributed to short-range coherence fundamentally attributed to the presence of particle-hole pairs.

According to Yi *et al.* [11], the Bragg peaks in the momentum distribution should narrow with a rise of the repulsive interactions in the system. However, the momentum density in Fig. 16 does not reveal this feature since even at extreme repulsion $a_c \sim O(1)$ the peaks have significant width. This is because the bosons are still able to hop between lattice sites to another generating a quasimomentum distribution [11]. The interactions have a finite range a_c which significantly reduces the localization effect as a_c becomes larger. It should be noted, that at very large a_c , such as $a_c = 2.00$, the only way the bosonic HSs can move around is by “turning around” each other.

Yi *et al.* also noted that an external harmonic trap broadens the momentum distribution of the bosons in an OL, particularly the condensate part. In fact, this is what is observed in Fig. 16.

G. Connecting with the work of Brouzos *et al.* [18]

In much relevance to our work, Brouzos *et al.* explored earlier 1D few bosonic systems in multiwell traps. They chiefly studied the effect of repulsive interactions on the distribution of particles in these traps. It was found, that for a 1D homogeneous multiwell trap with hard-wall boundaries and a commensurate filling factor (their) $\nu = 1$, the wells become equally occupied as the repulsion between the bosons rises [their Fig. 2(a)]. The particles thus tend to reduce their interaction energy by this rearrangement. In the weakly repulsive regime, and for a filling factor $\nu < 1$, i.e. an incommensurate filling, the particles are driven away from the central wells towards the outer wells and do not equally occupy the wells [their Fig. 10(a)]. In analogy to the latter result, we find that for an (although) inhomogeneous 3D OL with filling $N/N_L < 1$ (i.e. $\nu = N/N_L$), the particles are also driven away from the central well towards the outer lattice wells, particularly the corners of the CHOCL. The inset in their Fig. 10(b) shows how the populations of their wells change with the repulsion between the bosons. Most importantly, whereas the central site ($s = 4$) gets less populated as their g rises, the site ($s = 1$) farther away gets more populated. Our Figs. 3 and 5 display a similar behavior for the 3D CHOCL systems, although there does not seem to be a transfer of particles in the intermediate lattice wells between the central well of the CHOCL and its wells at the corners, as they reported. This is because none of the intermediate wells gains and subsequently loses population as those demonstrated by the inset of their Fig. 10(b).

In contrast to their 1D inhomogeneous result with $\nu > 1$ [their Fig. 14(a)], where even at large g the central wells remains significantly populated, the central cell of

the inhomogeneous 3D CHOCL becomes almost vacant! Thus, there is a higher tendency for the central well to become vacant in a 3D CHOCL than a 1D multiwell trap with harmonic confinement. As such, the dimensionality of this system seems to play a crucial role in this specific feature. This is particularly since the particles in 3D do not face the “energy obstacles” between the wells as much as in a 1D multiwell trap with harmonic confinement [18], when the tunnel from the center to the corners of the CHOCL. These “energetic obstacles” force the particles in a 1D inhomogeneous OL with $\nu > 1$ to favor the occupation of the middle wells.

For the filling factor $\nu < 1$, their particles remained delocalized and coherence did not vanish completely, contrary to the commensurate filling case. Our CHOCL systems with $\nu < 1$ are also incommensurately filled and as such will always display a delocalization of particles and an associated coherence manifested by a remaining SFF.

With regards to their momentum distributions in Fig. 11(c), they display a structure with Bragg peaks, where the central peak is lowered because of a partial loss of coherence with increasing repulsion between the bosons. Similarly, our Fig. 16 also displays a lowering of the central peak with increasing repulsion. The Bragg peaks surrounding the central one in our Fig. 16 reveal accordingly incomplete localization and persisting coherence, even as the system enters into the MI regime. In the work of Brouzos *et al.*, the Bragg peaks of the momentum distribution of a uniform 1D Bose gas in a multiwell trap with $\nu = 1$ vanish into a broad, smooth, Gaussian peak centered at $k = 0$ with a rise of g [their Fig. 5(a)].

Most importantly, Brouzos *et al.* computed the CF in the lowest natural orbital ($\ell = 0$) [their Fig. 11(b)] and showed how it declines with increasing g , whereas it rises for higher ones ($\ell > 0$). Our Figs. 3 and 5 display the same result for $\ell = 0$, where for (000), (001), and (010) the CF decreases. However, it rises for (011) and (111).

Our results for the 3D CHOCL with $\nu \neq 1$ are then very much in line with those of Brouzos *et al.* [18] for the 1D inhomogeneous case with $\nu \neq 1$.

IV. CONCLUSIONS

In summary, then, we have presented a numerical investigation of the CF and SFF of a few HC bosons in a 3D CHOCL of $3 \times 3 \times 3$ lattice sites. The global and local CF and SFF were computed for each CHOCL well and were explored as functions of a_c and the lattice wave vector $k = \pi/d$, d being the lattice spacing. The role of the interference between the condensates in all lattice wells, and its effect on the CF in one well was also studied. In a major part of this work, an achievement of a “pure” MI state was attempted, yet only mixed SF-MI phases were obtained.

The most important result of this paper is an opposing behavior for the global CF and SFF as functions of k . Whereas the global CF increases with increasing k , the

global SFF decreases with k . For the CF, this was explained by approximating each lattice well by a HO trap and the preference of the bosons to occupy the lowest HO level as the energy-level spacing increases with increasing k . For the SF, this was explained by an increase in the localization of the bosons in each lattice well as the local confinement strength increases with increasing k .

From a local perspective, it was found that the condensate is depleted with a rise of a_c in the lattice wells $\mathbf{R}_n \equiv (000)$, (001) , and (010) , whereas it rises with increasing a_c for (011) and (111) . This is because of the tunneling of the condensate away from the trap center to the farther lattice sites at the edges of the trap. The local CF is also enhanced with a rise of k in all lattice wells due to the same reasons outlined for the global CF. Further, when interference with all-neighbor sites is included, the CF in each lattice well is enhanced beyond the case with no interference effects. The local SFF as a function of a_c in each lattice well displays a similar behavior to the CF as it overall declines in the wells (000) and (010) whereas it rises in (011) and (111) . In contrast to the local CF, however, the local SFF decreases with increasing k , revealing again an opposing behavior to the CF on a local scale as well. An important point to mention, is that the local CFs and SFFs are of the same order of magnitude.

The energy of the system rises with an increase in a_c , largely because the average onsite interactions rise at a rate overwhelming the drop in kinetic energy, or mobility of the bosons. Further, the energy does not tend to stabilize towards a fermionization limit as it happens in the 1D homogeneous multiwell trap with commensurate filling $\nu = 1$ [18].

Finally, the possibility for achieving a “pure” MI state

in a 3D CHOCL with filling $\nu < 1$ was investigated in order to compare with the 1D homogeneous multiwell trap with hard-wall boundaries explored by Brouzos *et al.* [18]. This was performed by either increasing V_0 to 60 ($\hbar\omega_{ho}$) or by increasing a_c to huge values $a_c \sim O(1)$. It was found that no “pure” MI could be achieved in a 3D CHOCL, but rather a coexisting SF-(vacuum)MI phase. This is because for a filling $\nu < 1$, the particles remain delocalized and coherence cannot vanish completely even at huge a_c . From another point of view, the small number of $3 \times 3 \times 3$ sites does not furnish the ground for a flat MI density [13] to appear in the system. Consequently, our systems remain superfluid, even in the extreme repulsive regime with a global SFF of $\sim 20\%$ for $a_c \geq 2$. The presence of a global SFF does not guarantee the absence of local MI regimes, however. Further, the empty lattice wells in the CHOCL define vacuum MI regimes.

The momentum density of our systems with $\nu < 1$ reveals a broad central BEC peak surrounded by Bragg peaks, even at $a_c \sim O(1)$. This proves again the presence of a coexisting SF-MI phase in the extremely repulsive regime due to the delocalization of the particles. Thus, our results are in line with those presented by Brouzos *et al.* [18]. Had there been only one central BEC peak [26], the systems would have been defined as a “pure” MI.

Acknowledgments

ARS is indebted to the University of Jordan for funding this research project. Additional thanks go to William J. Mullin who earlier emphasized the importance of investigating the CF and SFF of the systems in Ref.[39] and also for a critical reading of the manuscript.

-
- [1] R. Bach and K. Rzazewski, Phys. Rev. A **70**, 063622 (2004).
 - [2] K. Xu, Y. Liu, D. E. Miller, J. K. Chin, W. Setiawan, and W. Ketterle, Phys. Rev. Lett. **96**, 180405 (2006).
 - [3] K. Sun, C. Lannert, and S. Vishveshwara, Phys. Rev. A **79**, 043422 (2009).
 - [4] Z. Chen and B. Wu, Phys. Rev. A **81**, 043611 (2010).
 - [5] A. Valizadeh, Kh. Jahanbani, and M. R. Kollahchi, Phys. Rev. A **81**, 023616 (2010).
 - [6] R. Ramakumar and A. N. Das, Phys. Rev. B **72**, 094301 (2005).
 - [7] H. Pu, L. O. Baksmaty, W. Zhang, N. P. Bigelow, and P. Meystre, Phys. Rev. A **67**, 043605 (2003).
 - [8] P. J. Y. Louis, E. A. Ostrovskaya, C. M. Savage, and Y. S. Kivshar, Phys. Rev. A **67**, 013602 (2003).
 - [9] N. Fabbri, D. Clément, L. Fallani, C. Fort, M. Modugno, K. M. R. van den Stam, and M. Inguscio, Phys. Rev. A **79**, 043623 (2009).
 - [10] S. Fang, R.-K. Lee, and D.-W. Wang, Phys. Rev. A **82**, 031601(R) (2010).
 - [11] W. Yi, G.-D. Lin, and L.-M. Duan, Phys. Rev. A **76**, 031602(R) (2007).
 - [12] D. van Oosten, P. van der Straten, and H. T. C. Stoof, Phys. Rev. A **63**, 053601 (2001).
 - [13] I. Hen, M. Iskin, and M. Rigol, Phys. Rev. B **81**, 064503 (2010).
 - [14] M. Rigol, G. G. Batrouni, V. G. Rosseau, and R. T. Scalettar, Phys. Rev. A **79**, 053605 (2009).
 - [15] I. Hen and M. Rigol, Phys. Rev. A **82**, 043634 (2010).
 - [16] J.-K. Xue, A.-X. Zhang, and J. Liu, Phys. Rev. A **77**, 013602 (2008).
 - [17] R. B. Diener, Q. Zhou, H. Zhai, and T.-L. Ho, Phys. Rev. Lett. **98**, 180404 (2007).
 - [18] I. Brouzos, S. Zöllner, and P. Schmelcher, Phys. Rev. A **81**, 053613 (2010).
 - [19] I. B. Spielman, W. D. Phillips, and J. V. Porto, Phys. Rev. Lett. **100**, 120402 (2008).
 - [20] A. A. Shams and H. R. Glyde, Phys. Rev. B **79**, 214508 (2009).
 - [21] D. Baillie and P. B. Blakie, Phys. Rev. A **80**, 033620 (2009).
 - [22] M. Greiner, O. Mandel, T. Esslinger, J. W. Hänsch, and I. Bloch, Nature **415**, 39 (2002).
 - [23] O. Gygi, H. G. Katzgraber, M. Troyer, S. Wessel, and G. G. Batrouni, Phys. Rev. A **73**, 063606 (2006).
 - [24] R. Roth and K. Burnett, Phys. Rev. A **67**, 031602(R)

- (2003).
- [25] D. Tilahun, R. A. Duine, and A. H. MacDonald, *Phys. Rev. A* **84**, 033622 (2011).
- [26] I. Hen and M. Rigol, *Phys. Rev. B* **80**, 134508 (2009).
- [27] B. Capogrosso-Sansone, E. Kozik, N. Prokof'ev, and B. Svistunov, *Phys. Rev. A* **75**, 013619 (2007).
- [28] J. Li, Y. Yu, A. M. Dudarev, and Q. Niu, *New J. Phys.* **8**, 154 (2006).
- [29] M. J. Hartmann and M. B. Plenio, *Phys. Rev. Lett.* **100**, 070602 (2008).
- [30] F. Gerbier, A. Widera, S. Fölling, O. Mandel, T. Gericke, and I. Bloch, *Phys. Rev. A* **72**, 053606 (2005).
- [31] M. Yamashita and M. W. Jack, *Phys. Rev. A* **76**, 023606 (2007).
- [32] M. Capello, F. Becca, M. Fabrizio, and S. Sorella, *Phys. Rev. Lett.* **99**, 056402 (2007).
- [33] S. Ramanan, T. Mishra, M. S. Luthra, R. V. Pai, and B. P. Das, *Phys. Rev. A* **79**, 013625 (2009).
- [34] A. Rancon and N. Dupuis, *Phys. Rev. A* **85**, 011602(R) (2012).
- [35] G. G. Batrouni, V. Rosseau, R. T. Scalettar, M. Rigol, A. Muramatsu, P. J. H. Denteneer, and M. Troyer, *Phys. Rev. Lett.* **89**, 117203 (2002).
- [36] T. Stöferle, H. Moritz, C. Schori, M. Köhl, and T. Esslinger, *Phys. Rev. Lett.* **92**, 130403 (2004).
- [37] M. Snoek, I. Titvinidze, I. Bloch, and W. Hofstetter, *Phys. Rev. Lett.* **106**, 155301 (2011).
- [38] G. E. Astrakharchik and K. V. Krutitsky, *Phys. Rev. A* **84**, 031604 (2011).
- [39] A. R. Sakhel, J. L. DuBois, and R. R. Sakhel, *Phys. Rev. A* **81**, 043603 (2010).
- [40] J. L. DuBois and H. R. Glyde, *Phys. Rev. A* **63**, 023602 (2001).
- [41] E. L. Pollock and D. M. Ceperley, *Phys. Rev. B* **36**, 8343 (1987).
- [42] For this purpose, we modified a VPI code previously written by Jonathan L. DuBois which he has given us earlier.
- [43] J. E. Cuervo, P.-N. Roy, and M. Boninsegni, *J. Chem. Phys.* **122**, 114504 (2005).
- [44] M. H. Kalos and P. A. Whitlock, *Monte Carlo Methods, Volume I: Basics* (John Wiley and Sons, 1986).
- [45] G. B. Arfken and H. J. Weber, *Mathematical Methods for Physicists* (Academic Press, San Diego, USA, 1995), 4th ed.
- [46] I. B. Spielman, W. D. Phillips, and J. V. Porto, *Phys. Rev. Lett.* **98**, 080404 (2007).
- [47] A. R. Sakhel, J. L. DuBois, and H. R. Glyde, *Phys. Rev. A* **77**, 043627 (2008).
- [48] William J. Mullin, University of Massachusetts, Amherst MA, USA. Private communications.
- [49] D. Jaksch, C. Bruder, J. I. Cirac, C. W. Gardiner, and P. Zoller, *Phys. Rev. Lett.* **81**, 3108 (1998).
- [50] Marcos Rigol, Department of Physics, Georgetown University, Washington DC, USA. Private communications.
- [51] W. J. Mullin, *J. Low. Temp. Phys.* **106**, 615 (1997).
- [52] G. V. Chester, in *Lectures in Theoretical Physics*, edited by K. T. Mahanthappa (Gordon and Breach, Science Publishers, Inc., New York, 1968), p. 253.
- [53] G. V. Chester, M. E. Fisher, and N. D. Mermin, *Phys. Rev.* **185**, 760 (1969).
- [54] F. Gerbier, A. Widera, S. Fölling, O. Mandel, T. Gericke, and I. Bloch, *Phys. Rev. Lett.* **95**, 050404 (2005).